PRODUCTION ALTERNATIVES TO SCREEN PRINTING FOR DYE SENSITIZED SOLAR CELLS IN LABORATORY SETTINGS

A Thesis by

Holly Haynes

Bachelor of Science, Wichita State University, 2007

Submitted to the Department of Mechanical Engineering
and the faculty of the Graduate School of
Wichita State University
in partial fulfillment of
the requirements for the degree of
Master of Science

December 2010

PRODUCTION ALTERNATIVES TO SCREEN PRINTING FOR DYE SENSITIZED SOLAR CELLS IN LABORATORY SETTINGS

The following faculty members have examined the final copy of this thesis for form and content, and recommend that it be accepted in partial fulfillment of the requirement for the degree of Master of Science with a major in Mechanical Engineering.

_____
Ramazan Asmatulu, Committee Chair

_____
Hamid Lankarani, Committee Member

_____
Paul Rillema, Committee Member

DEDICATION

To my family and friends.

Experience: that most brutal of teachers. But you learn, my God do you learn.

ACKNOWLEDGMENTS

I would like to thank my advisor and committee chair, Dr. Ramazan Asmatulu, for his unfailing support and guidance throughout this project. I would also like to extend my gratitude to the members of my committee, Dr. Hamid Lankarani and Dr. Paul Rillema, for their helpful comments and suggestions on this project. Dr. Francis D"Souza and Navaneetha Subbaiyan of the Chemistry Department of Wichita State University provided invaluable help in the form of information and access to testing facilities used in this project. I must express my thanks to Dr. Nurxat Nuraje of the Department of Materials Science and Engineering at MIT for advice and testing, to Dr. James Ho of the Physics Department of Wichita State University for arranging the characterization of materials related to this thesis, and to Heath Misak for arranging microscope images. I appreciate the assistance of Daouda Diouf in preparing samples. Thanks also to Manish Shinde, my fellow researcher, for his significant contributions to our work.

ABSTRACT

In this thesis, two methods of creating multi-layer porous films for DSSCs are examined. They have been designed as possible alternatives for screen printing in laboratory settings. The same precursor chemicals used for screen printing are employed in both the alternative methods, which are designated multi-layer doctor-blading and stamping. Both alternatives are simple and inexpensive, costing $0.86 and $0.89 per DSSC, respectively. Multi-layer doctor bladed cells can be made with up to three layers, while stamped cells can be made with up to eight.

The cells produced by these two methods are compared to a sample screen printed cell, with mixed results. The multi-layer doctor bladed cells exhibit lower current densities than a screen printed cell, 68.0 A/m^2 compared to 68.9 A/m^2. The best performing stamped cell demonstrates a higher current density than the screen printed reference, reaching 82.7 A/m^2. It also has a slightly higher efficiency. However, the results from the stamped cells are inconsistent. In order for it to truly become an effective method for creating DSSCs in laboratory settings, the source of this variation must be found and standardized.

TABLE OF CONTENTS

TABLE OF CONTENTS (continued)

LIST OF TABLES

LIST OF FIGURES

LIST OF FIGURES (continued)

LIST OF FIGURES (continued)

LIST OF ABBREVIATIONS/NOMENCLATURE

AM	Air Mass
DSSC	Dye Sensitized Solar Cell
IPCE	Incident-Photon-to-Current Efficiency
LHE	Light Harvesting Efficiency
TCO	Transparent Conducting Oxide
FF	Fill Factor

LIST OF SYMBOLS

E_G	Band Gap Energy
η_c	Collection Efficiency
E_C	Conduction Band Minimum Energy
ρ	Density of Holes
m_e	Effective Electron Mass
k_{inj}	Electron Injection Coefficient
eV	Electron Volts
t_f	Excited State Lifetime
I_L	Initial Current Generated
λ	Light Wavelength
I_{MP}	Maximum Power Current
P_{MP}	Maximum Power Generated
V_{MP}	Maximum Power Voltage
Φ	Monochromatic Light Intensity
V_{OC}	Open Circuit Voltage
η	Overall Efficiency
E_λ	Photon Energy
π	Pi
h	Planck‟s Constant
φ_{inj}	Quantum Yield of Electron Injection
I_{SC}	Short Circuit Current
J_{SC}	Short Circuit Current per Unit Area
c	Speed of Light
P_{IN}	Sunlight Inherent Power
E_V	Valence Band Maximum Energy

CHAPTER 1

INTRODUCTION

1.1 Background

Sunlight is the most abundant energy source on the planet. It is also the only net energy input into the otherwise closed system of Earth. Photovoltaic technologies use sunlight to produce electrical energy. Semiconductors in photovoltaic devices absorb photons present in the light rays and generate DC current that can be stored or used to drive electrically powered devices [1]. The ability of photons to cause electron movement is called the photoelectric effect. It was first described by Alexander Becquerel in 1839 [2]. The first successful photovoltaic device, composed of selenium coated in gold leaf, emerged in 1883. Bell Labs created the first economically feasible solar cell in 1954 from silicon. This cell boasted a 6% efficiency. Over the next twenty years, researchers worldwide refined the understanding of solar cell physics, exploring concepts such as efficiency and material selection. By 1973, solar cells had been deemed sufficiently viable to warrant government funding [1].

Photovoltaic research continues to advance, and new technologies are being explored. One such alternative photovoltaic device is the dye sensitized solar cell (DSSC, sometimes DSC). Cells of this type capture solar energy in a dye, and through electron transfer between the dye and a semiconductor, create a usable current [3]. This process mimics photosynthetic plants, which use pigments like chlorophyll to channel solar energy into complex chemical reactions [4].

1.2 Goals

This thesis will examine the origins of DSSCs and the science that drives them. The standard anatomy and constituents of a DSSC will be summarized, as well as the typical construction procedures employed in the cells‟ creation. Building on this initial information, the

subsequent attempts by the author to develop alternative methods for creating multi-layered DSSCs will be detailed. Finally, the outcomes of these alternate methods will be analyzed and discussed.

CHAPTER 2

LITERATURE REVIEW OF DSSCS

2.1 Dye Sensitized Solar Cell History

The majority of the manufacturing and research during the history of photovoltaic development has been focused on solar cells composed of single crystalline semiconductor sheets. These products dominate the photovoltaic market, holding 94% of the market share [5]. However, in parallel to the development of the standard cell, progress has been made toward the modern DSSC. The first widespread use of dye sensitized metal occurred in photography, or more specifically, daguerreotypy. This process, invented in 1840, created images by focusing light on a silver plate coated in iodine and bromine [6]. An example appears in Figure 1.

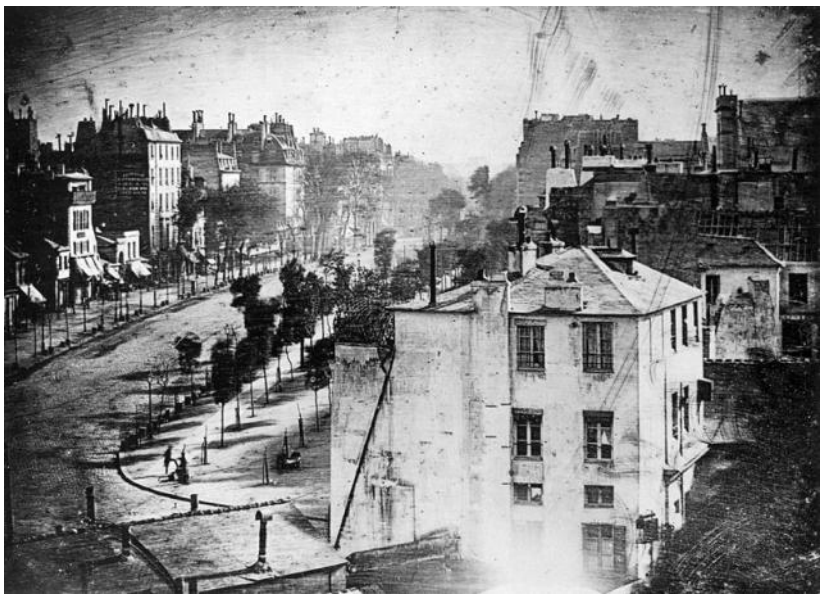

Figure 1: Early daguerreotype image [6].

In 1887, James Moser documented the ability of dye to increase the photovoltaic effect on silver [4]. In 1977, Matsumura et. al. worked with indium coated zinc oxide and rose bengal dye. They determined the mechanism by which dye absorbed onto the surface of an electrode promotes electron transfer. Previously, the exact mechanism by which electrons were transferred

and to and from the dye had been debated. In particular, they proved that only dye in contact with the electrode generates current, and that dye in solution is not useful [7]. Subsequent researchers continued to use ZnO, as well as SnO_2, semiconductors in combination with dyes. However, few of these cells managed an efficiency over 1%, and were therefore unable to rival silicon cells [3].

In 1991, researchers Brian O'Regan and Michael Grätzel (sometimes listed at Graetzel) published an article in Nature magazine detailing their creation of a DSSC that achieved 7.12% to 7.9% efficiency in direct sunlight. O'Regan and Grätzel also observed that their DSSC proved more efficient in the presence of indirect light, reaching 12% efficiency [3]. Grätzel had been working in solar cell research for some time when he was approached by O'Regan about a thin, porous TiO_2 film that was being investigated for its filtration properties. O'Regan suggested that this film might prove successful as a semiconductor for DSSCs. Grätzel agreed, and the two collaborated to produce the most efficient DSSC that had as yet been created [4]. This advance was a remarkable leap forward for the DSSC, so much so that the term DSSC and "Grätzel Cell" are sometimes used synonymously.

2.2 Solar Cell Principles

The science involved in energy generation through DSSCs is cross-disciplinary, involving chemistry, optics, and quantum mechanics. A brief description of the process and the principles that govern it follows.

2.2.1 Light Harvesting Principles

The energy in sunlight is stored in particles called photons which have no mass. The energy carried by each photon is determined by the wavelength of the light. The lower the wavelength, the greater the energy the light carries. Visible light has wavelengths between 400

and 700 nm, and these are the wavelengths from which dye-sensitized solar cells derive energy. When a photon interacts with an atom, it can be absorbed, transferring its energy to a valence electron. If the energy in the photon is sufficient, it can cause a quantum leap, forcing the electron out of its orbital. Equation (1.1) shows the relationship between the energy contained in a photon, E_λ, Planck"s constant h, and the speed of light, c.

$$E_\lambda = {}^{hc}/_{\lambda} \tag{1.1}$$

It is clear from equation (1.1) that the energy of a photon is inversely dependent on the wavelength of the light in which it may be found, so that the lower the wavelength, the more energetic the particle [8].

In metals and semiconductors, an electron pushed out of the valence band enters the conduction band, and a current is created [8]. Metals have overlapping conduction and valence bands, whereas semiconductors have a separation between their conduction and valence bands [9]. Figure 2 illustrates this region for what is known as a direct band-gap semiconductor. Between the valence band maximum energy, E_V, and conduction band minimum energy, E_C, lies the band gap. The "width" of this band varies based on individual material properties. The minimum energy required to displace the electron, E_G, is referred to as the band gap energy. An electron needs to absorb a greater amount of energy to cross a larger band gap. Thus, band gap energy is an indicator both of the photovoltaic activity and of the conductivity of the semiconductor.

In the case of indirect band gap semiconductors, such as silicon, the nature of the crystal lattice in the semiconductor causes the two curves to be out of phase. This means that the maximum and minimum are no longer aligned, and that an electron whose energy has been increased does not automatically enter the conduction band without a crystal lattice vibration.

Such vibrations can be idealized as a particle called a phonon. The release or absorption of a phonon allows the electron to translate into the conduction band after excitation [8, 9]. This process is illustrated in Figure 3. Because indirect band gap semiconductors require an extra step in the energy generation process, they are theoretically less efficient than direct band gap materials [9].

After an electron is transferred to the conduction band, it leaves behind a hole. This hole can be represented as a local positive charge. A hole is filled when an electron drops from the conduction band into the valence band, a phenomenon called recombination. This event is triggered by a release of energy by an excited electron, often when it encounters a crystal lattice defect or a grain boundary. Such an event dissipates the energy as heat. Recombination may also occur when energy is emitted as radiation from the cell [8].

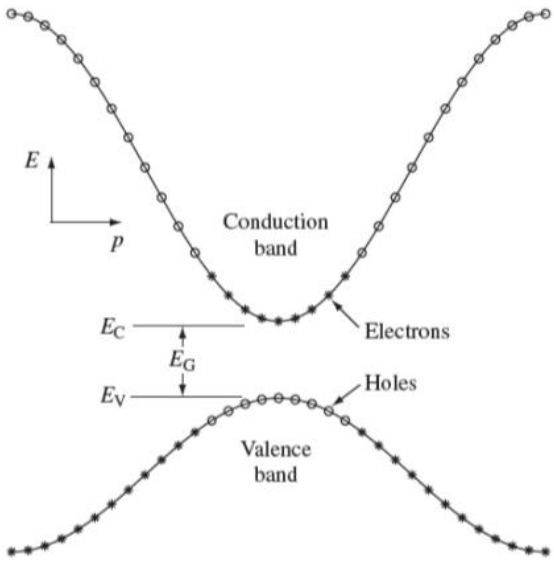

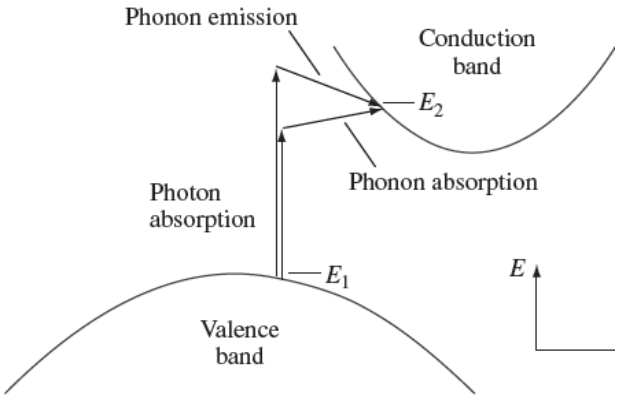

Figure 2 (left): Illustration of electron transfer between the valence and conduction bands [8].
Figure 3 (right): Illustration of electron transfer between offset valence and conduction bands, necessitating the release or absorption of a phonon [8].

In order to channel the energy imparted by the photons to the semiconductor, it is necessary to separate the positive and negative charges within the material. In a traditional

photovoltaic cell, this requires the layering of n- and p-type materials. An n-type material has been treated, or doped, in such a way that it contains more negative charges than it contains positive charges. The added electrons in the material are highly mobile, and when excited into the conduction band, they do not create a hole. A p-type material receives the opposite kind of doping: it contains more positive charges than negative charges. Figure 4 shows a cross-section of a standard cell. The sandwiching of p- and n-type materials in this manner creates a pn junction in which the different electric potentials induce an electromagnetic current across the cell. The current directs the movement of both holes and electrons within the semiconductor; electrons move in opposition to the current and holes move with it [8, 9]. A metal grid at the top of the solar cell and a contact at the back of the cell allow a circuit to be formed and carry current to and from the device [8].

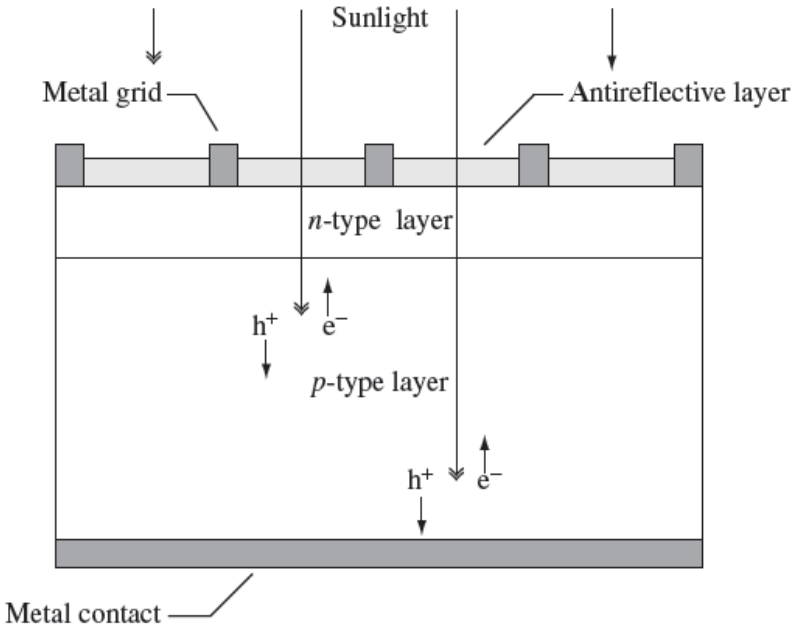

Figure 4: Schematic of a traditional solar cell featuring p- and n-type materials [8].

The semiconductors used for the variety of cell described above have relatively small band gaps. The ideal band gap for a solid, semiconductor photovoltaic cell is considered to be

1.1 eV. For silicon, the band gap is around 1.12 eV, near perfect [10]. While silicon is itself an elemental semiconductor, composite semiconductors containing atoms of a metal and nonmetal are often created to achieve a similar band gap. Figure 5 shows the valence and conduction bands of three semiconductors and their band gaps. Gallium arsenide, at left, is a composite direct band gap semiconductor with an E_G of 1.42 eV. Like silicon, it has been effectively used in solar cells. Germanium, at right, is another elemental semiconductor with the unusual property of having two viable band gaps, one direct and one indirect, and therefore two E_G, 0.66 and 0.9 eV [9].

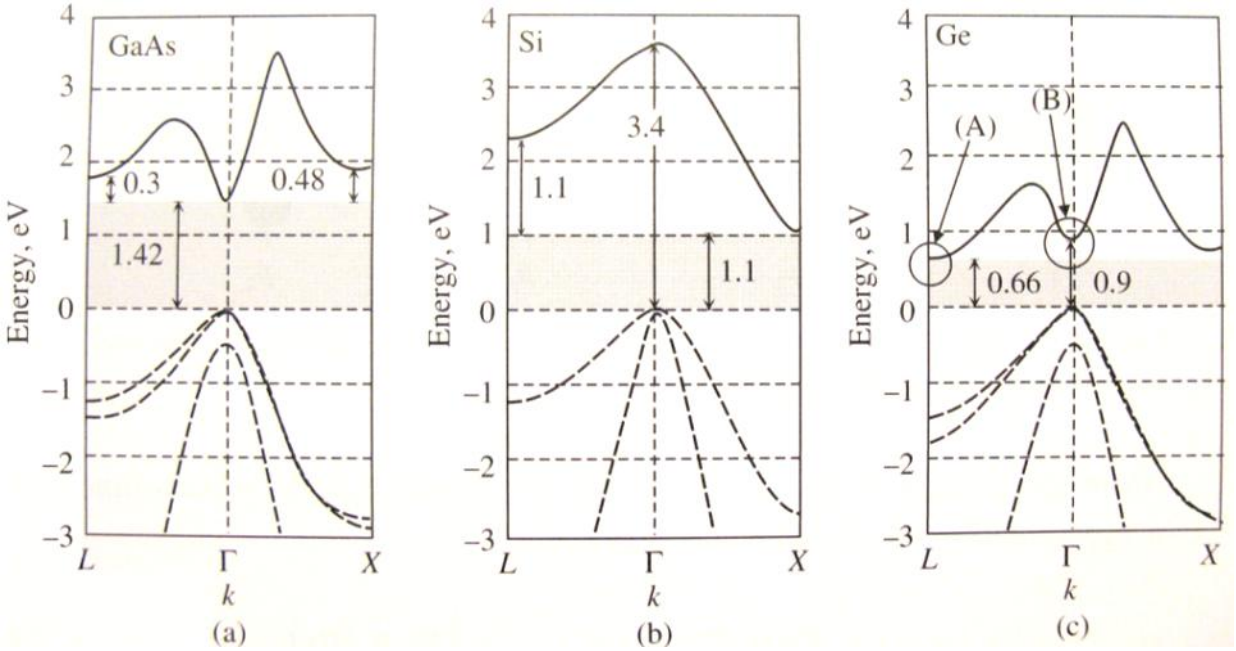

Figure 5: Conduction band energies for (a) GaAs, (b) Si, and (c) Ge [9].

A material with a wide band gap will not generate photovoltaic energy on its own because the photons in visible light lack the energy needed to excite its electrons [10]. However, that does not preclude the use of that material in a solar cell. In traditional cells, the absorption of photons and the transmission of energy take place in the same material. But if two materials are used in conjunction, one of them light sensitive and one of them a conductor, the functions

can be separated. Photons can enter a coating on a wide band-gap semiconductor and displace the coating‟s electrons, which are then free to enter the semiconductor and create a current. DSSCs employ a light absorbing dye as the coating material [3, 10]. A dye, or sensitizer, has only a limited number of electrons that it can pass on to an electrode. If no additional electrons are supplied to the dye, the current flowing through the cell will soon cease. In order to complete the DSSC circuit, electrons must be returned to the dye [7].

This means that a complete circuit must be created. As with standard photovoltaic cells, two electrodes are required, one to transmit current out of the cell and one to return it to the dye [10]. The photo-electrode consists of a film of the selected semiconductor deposited on a conducting substrate. Often, a sheet of transparent conducting oxide glass (TCO glass) is used as a base for film construction. This glass has been pretreated with a clear semiconductor so that it can transmit current. Electrons pass from the dye to the photo-electrode, travel through the circuit outside of the solar cell, and then re-enter at the counter-electrode. The counter-electrode is placed on top of the dye; depending on the illumination source, it may be between the dye and the light. For this reason, it must be composed of a clear material; this necessitates the use of another sheet of TCO glass for the counter-electrode [10, 11]. Because the surface of the semiconductor film is porous, a subject that will be discussed in more detail in later sections, the dye molecules that need to be regenerated are not located on a plane. As a result, the flat surface of the counter-electrode cannot make contact with all of the dye molecules, so a liquid electrolyte is used to sustain a redox reaction that recharges the dye [3, 12].

A redox reaction is a chemical process that occurs when electrons are transferred between reactants. The term redox is short for “oxidation-reduction.” The oxidation half reaction occurs when one of the reactants, the reducing reactant, donates an electron. The reduction half reaction

occurs when the second reactant, the oxidizing reactant, receives the electrons given off in the first half-reaction [13]. In DSSCs, the molecules in the electrolyte are oxidized at the dye and then reduced when they make contact with the counter-electrode. In theory, this process can be repeated an infinite number of times, as with a catalytic reaction [4, 10].

Plate 1 in Appendix A shows a detailed schematic of a DSSC constructed from a thin, porous TiO_2 semiconductor film with an iodide/triiodide redox couple. A scale is not given for this image, but the thickness of semiconductor films in this type of cell arrangement is typically measured in nanometers. The images show representations of light entering a cell, electron flow rate, and the redox reaction. As illustrated in the magnified inset of the TiO_2 film, the electrolyte pervades the cell. It should be noted that both the dye and electrolyte molecules are far smaller than the semiconductor pores; this allows for widespread dye penetration of the semiconductor [10].

2.2.2 Solar Cell Efficiencies

In the assessment of solar cell performance, it is standard practice to use light at AM 1.5. The term AM stands for air mass, which is calculated using the equation (1.2), where θ represents the incident angle of solar rays striking the surface of a solar cell.

$$AM = {}^{1}/_{\cos(\theta)} \tag{1.2}$$

This value allows researchers to account for the amount of light absorption that occurred in the atmosphere before the light reached the cell. Figure 6 diagrams the wavelengths versus the incident power for three different sources. The top curve represents black body radiation at a temperature of 5762 K. The middle curve, labeled AM0, reflects the solar spectrum as it would be measured just outside the Earth‟s atmosphere [8]. The bottom curve, AM 1.5g, represents light that has passed through approximately 1.5 air masses [11]. The “g” listed next to the AM

1.5 label stands for global. This means that all light, both that which lands directly on the cell and that which is reflected back to the cell from the environment, are considered. If a "g" were replaced by a "d", it would mean that only direct sunlight was considered and that diffuse light sources were omitted [8].

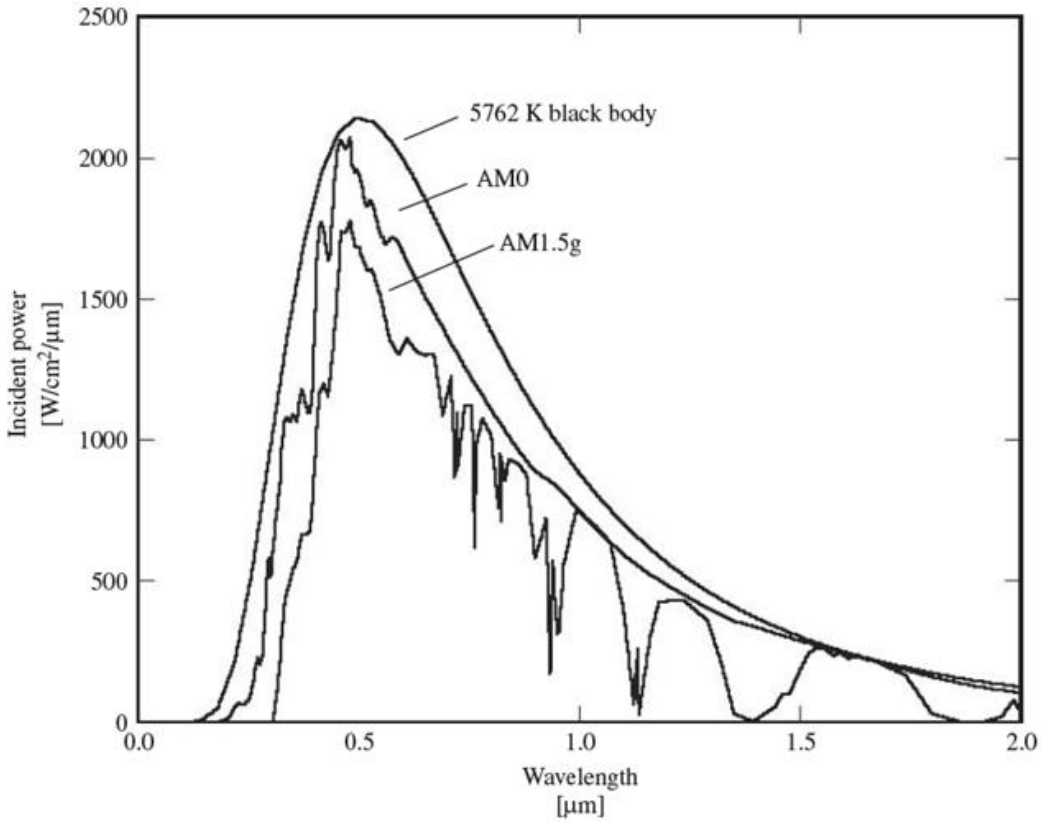

Figure 6: Spectra of light measured at different locations and angles [8].

Using a standardized light spectrum allows the attributes of cells created from different methods to be compared. Several characteristics can be used to describe a solar cell, whether it is a traditional photovoltaic or a DSSC. These include the open circuit voltage (V_{OC}), short circuit current (I_{SC}), maximum power voltage (V_{MP}), and maximum power current (I_{MP}). It can be helpful to explain these factors in terms of a graph of a solar cell"s current versus voltage. A typical curve is shown in Figure 7, complete with sample values. The V_{OC} is the maximum potential voltage across a cell, which is observed only when the rate of electron recombination

and the rate of current generation are equivalent; this means that there is no net current in the system. The I_{SC} is the maximum current that can be generated by the cell. As shown in the graph, it is constant over a wide range of voltages, but deteriorates as the cell voltage approaches its peak. Sometimes, short circuit current density, J_{SC}, and current density, J, are used instead of I_{SC} and current, I, to compare cells of different areas. These values are calculated by dividing I_{SC} and I by the cell‟s working surface area. The power generated by a cell at a certain point on the current/voltage curve can be calculated by multiplying the voltage and current coordinates of the point. The V_{MP} and I_{MP} correspond to the point on the curve where the maximum power, P_{MP}, is generated. It is clear that cell operation should be maintained as close to this point of the curve as possible [8, 11].

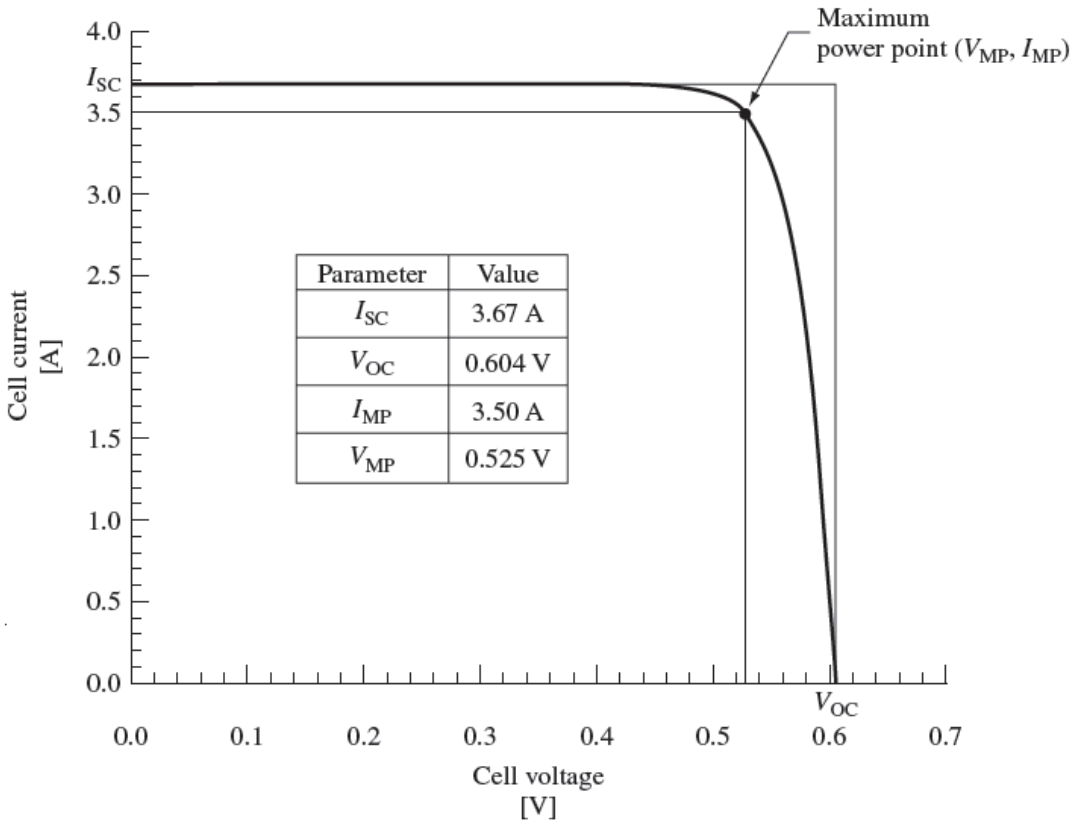

Figure 7: Current vs. voltage for an example solar cell [8].

The fill factor (FF) of a solar cell has been described as a measure of how closely the area under the current/voltage curve corresponds to an ideal rectangle, and is an indicator of internal efficiency. It may be given as a percentage less than 100% or as a decimal less than 1.0. Equation (1.3) shows how the FF is calculated.

$$FF = {}^{P_{MP}}/_{V_{OC}I_{SC}} = {}^{V_{MP}I_{MP}}/_{V_{OC}I_{SC}} \tag{1.3}$$

The overall efficiency of a solar cell, η, is a ratio of the power produced by the cell to the inherent power in the sunlight that impacts the cell, P_{IN}. The value of P_{IN} is often determined experimentally. Efficiency is calculated using equation (1.4) [8].

$$\eta = {}^{P_{MP}}/_{P_{IN}} = {}^{V_{OC}I_{SC}FF}/_{P_{IN}} \tag{1.4}$$

In addition to efficiency as defined above, there are a variety of internal efficiencies often calculated for solar cells. One of these is the light harvesting efficiency (LHE) of a cell, which measures the ability of a cell to absorb photons. It is frequently used to describe the effectiveness of the dyes used in DSSCs. The means of calculating LHE are listed in equation (1.5), where the variable A represents the absorbance of the dye and the variable T represents the transmittance of the dye [10].

$$LHE = 1 - T = 1 - 10^{-A} \tag{1.5}$$

The collection efficiency of a cell, η_c, illustrates the number of electrons excited in the cell that manage to move through the photo-electrode and out of the cell. It is the ratio in equation (1.6), where I_L represents the current that is initially generated by the photons hitting the cell before recombination losses occur [8].

$$\eta_c = {}^{I_{SC}}/_{I_L} \tag{1.6}$$

The LHE and the collection efficiency can be used to calculate the incident photon-to-current efficiency (IPCE) of a DSSC. This represents the percentage of the photons that are absorbed by the cell and contribute to useful current production. The formulas for IPCE are shown in equation (1.7). The variables in the first equality must be measured using monochromatic light of wavelength λ. The term J_{SC} stands for the short circuit current of the cell per unit area, or short circuit current density. The variable Φ represents the monochromatic light intensity. In the second equality, φ_{inj} represents the quantum yield of electron injection [10].

$$IPCE = {(1240\ eV \cdot nm)J_{SC}}/{\lambda\Phi} = LHE\varphi_{inj}\eta_c\eta_c = {I_{SC}}/{I_L} \qquad (1.7)$$

These efficiencies are an essential part of solar cell research because they document energy loss during the photovoltaic process. In general, energy losses within a cell follow the pattern given in Figure 8. Efforts to improve DSSCs aim to reduce the efficiency drop occurring at one or more of the stages listed.

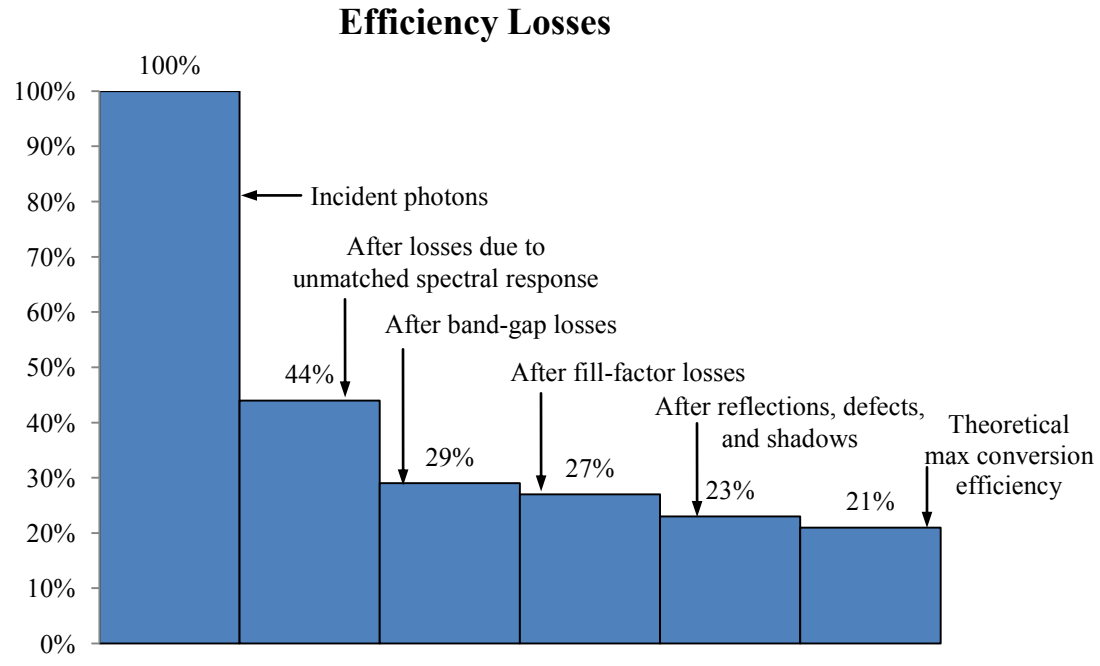

Figure 8: Efficiency losses incurred during cell operation [5].

The maximum possible efficiency of a traditional photovoltaic device was calculated in 1961 to be 32%; this is referred to as the Shockley-Queisser Limit [11]. This limit assumes the use of no light concentrators and no series or parallel cell combinations [8, 11]. Other estimates, such as the 21% efficiency given in Figure 8, vary depending on the type of cell being analyzed and the range of light it is expected to harvest. The average efficiency of a monocrystalline silicon cell is 14 to 17% when produced commercially. In a laboratory setting, it can climb to 24% or higher, but these conditions are difficult to replicate on a large scale [2]. For DSSCs, average efficiency is much lower; the record efficiency is presently 11.3%, set in 2008 using titania paste [14]. At present, the record efficiency achieved by any photovoltaic cell is 41.1%, a benchmark set by the Fraunhofer Institute of Solar Energy Systems (ISE) in Germany with a GaInP/ GaInAs cell [15].

2.3 Cell Components

DSSCs contain four major components: the semiconductor material that transmits the electrical current, the dye that sensitizes the cell, the electrolyte that recharges the dye, and the conducting glass that acts as the second electrode. Proper selection of each material is vital in maximizing cell efficiency.

2.3.1 Semiconductors

Early efforts to create dye-sensitized solar cells managed to generate current, but with minimal efficiencies, most around 1%. Researchers used pure semiconductor materials melted and formed into plates with large single crystals to minimize lattice defects. This step had been critical in standard solar cells to avoid light scattering and recombination [10]. However, in DSSCs a smooth semiconductor surface prevents the dye from being absorbed, and limits the points at which dye molecules may attach to the semiconductor [3]. It was found that the efficiency of DSSCs could be dramatically increased through the use of a porous semiconductor

film, as shown in Figure 9 [13]. A thin, porous metal substrate can feature 100 to 1000 times the surface area of a smooth film with the same length and width. With DSSCs, the greater the metal surface area, the more dye interaction possible, and the greater the electric current that can be generated. Also, the random orientation of the particles in the film can cause light scattering, increasing the potential for those light rays that were not absorbed by the dye to be redirected toward other dye molecules [4].

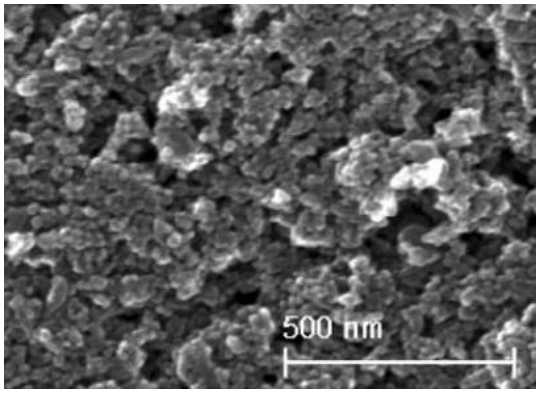

Figure 9: Porous TiO_2 film [16].

Traditional solar cells employ semiconductors such as silicon, gallium arsenide, indium phosphide, and cadmium sulfide. While effective semiconductors in the absence of dye, these materials are not practical for dye sensitized cells. The presence of liquid components in the cell, the dye and the electrolyte, combined with the energy input of the absorbed photons leads to photocorrosion. Once the surface of the electrode is corroded, electrical conductivity is no longer feasible. To solve this problem, heavy metal oxides are employed, such as SnO_2 and ZnO. While stable, these semiconductors were not used for light harvesting purposes in first generation solar cells because they have wide band gaps, and cannot generate useful current on their own. However, with a sensitizer, they can become effective [10]. In the 1991 article by O'Regan and Grätzel, TiO_2 was proposed as a suitable semiconductor, and their porous films produced a 7.12 to 7.9% efficiency as previously stated [3].

Of the three material options given, TiO_2-based cells have yielded higher average efficiencies than those composed solely of SnO_2 and ZnO. It has been suggested that the disparity is due to the differences in electron mobility in the materials. The disparity can be assessed using the wave function of the electrons, which is dependent on the effective masses of the particles. Effective mass takes into account the forces exerted on electrons by the atoms and particles surrounding them as they move. For ZnO and SnO_2, the effective electron masses are 0.2 m_e and 0.1 m_e. For TiO_2, the effective mass is as high as 10 m_e. This high effective mass appears to limit recombination losses, preventing the electrons from being reabsorbed before the current can be transmitted. In theory, the higher the effective mass of a semiconductor's electrons, the more efficient it may be for use in DSSCs [17]. So, in spite of TiO_2's relatively low electron mobility, around 10^{-5} $cm^2/V \cdot s$, compared to 115 $cm^2/V \cdot s$ for ZnO, TiO_2 is the more useful material for this application [18].

To further augment the transmission abilities of TiO_2, hybrid film structures can be created. TiO_2 has a variety of crystal structures, and its band gap of varies depending on the lattice arrangement that dominates the sample. The two most common forms of TiO_2 are anatase and rutile, with respective band gaps of 3.2 and 3.02 eV [19]. Of the two, rutile is the more common and the less expensive. Both occur in a tetrahedral crystal structure, but anatase has a more complex unit cell. A comparison of the two structures can be seen in Figure 10. Research suggests that anatase has superior properties for DSSC applications [13], but rutile can also be used. Combining both varieties in a DSSC can produce a more efficient cell than rutile alone [16]. Whether nanoparticle films are primarily rutile or primarily anatase depends on the manufacturing method; in a hybrid rutile/anatase sample, the band gap is an intermediate value between the band gaps of the pure crystal structures.

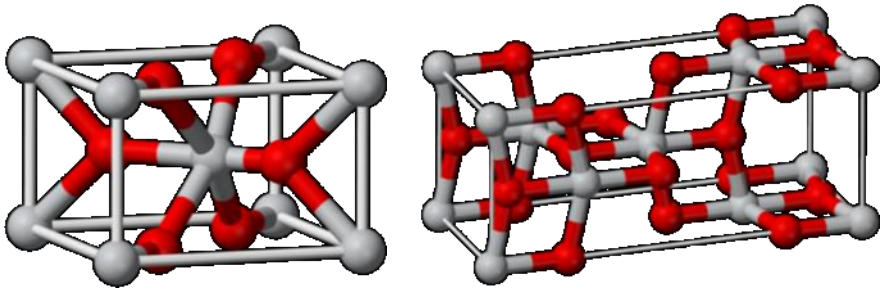

Figure 10: Unit cells of rutile (left) [20], and anatase (right) [21].

The properties of a semiconductor film can be altered by doping or modifying with another type of molecule. A variety of substances have been added in an attempt to improve the conductivity of TiO_2 films. These materials can be aimed at light scattering, increasing current, or reducing the material band gap in an attempt to harvest longer light wavelengths. Attempts to improve TiO_2 properties have been made with materials as common as nitrogen [22] and as exotic as neodymium [23].

2.3.2 Dye

The two functions of the dye in a DSSC are to absorb photons and to transfer current to the semiconductor substrate. The ideal dye, or sensitizer, used in the construction of DSSCs should have a wide absorption spectrum. The wider the spectrum, the more energy generation potential the dye has. Most solar energy is derived from waves in the visible light range, with wavelengths from roughly 400 to 700 nm, but with some dyes it is possible to generate energy in the near-infrared spectrum, ~900 nm [24]. It should be noted that energy absorption cannot be increased by adding additional dye to the cell. Only the molecules in direct contact with the semiconductor film can transmit electrons. Any molecules of dye that overlap interfere with one another‟s ability to take in light, so excess dye can in fact decrease a cell‟s efficiency [4]. Also, if the dye contains large molecules, one molecule can prevent other molecules from accessing some of a film‟s interior pores [3].

In order to adhere to the surface of a semiconductor, a dye should contain either a carboxylate or phosphonate group [13, 24] or a catechol moiety [4]. These groups provide an overlap between the conduction band of the semiconductor and the exited state orbital of the dye, allowing free electron transfer [4]. The interaction of these functional groups with the semiconductor can create a local positive charge at the surface. This slight charge can help motivate electrons to move from the dye molecules to the thin film in what is termed ligand-to-metal charge transfer [4]. Figure 11 illustrates these chemical groups.

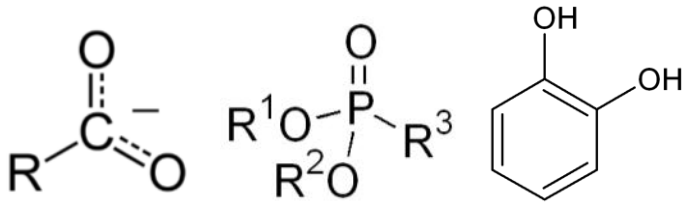

Figure 11: From left to right, carboxylate [25], phosphonate [26], and catechol[27].

A wide variety of dyes can be used for DSSCs. One dye frequently employed in early DSSC research was rose bengal [7], the structure of which appears in Figure 12. This medical dye is often used as a stain on microscope slides. Its absorption spectrum appears in Figure 13.

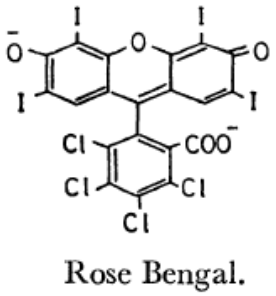

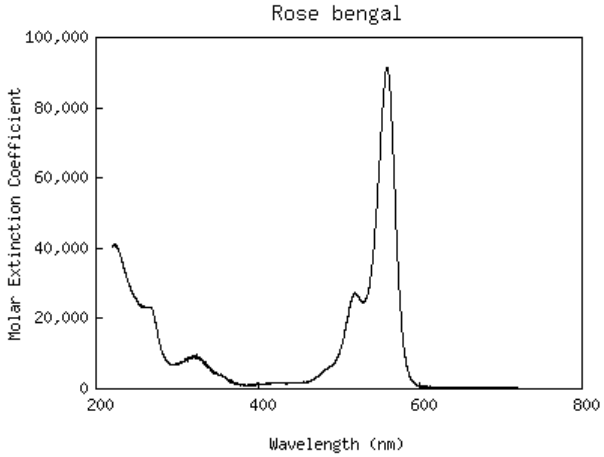

Figure 12 (left): Chemical structure of rose bengal [7].
Figure 13 (right): Absorption spectrum of rose bengal [28].

Rose bengal has a narrow absorption spectrum, with the highest peak occurring between 450 and 600 nm [28]. This limited the effectiveness of cells made with this and similar dyes [13]. Semiconductor films are more efficient with some dyes than with others. ZnO films work well with merbromin, and SnO_2 film absorption can be improved by the use of indolin [17]. To broaden the absorption spectrum of cells, most researchers have turned to ruthenium based dyes. Four such dyes are listed in Table 1, along with other dyes employed for DSSCs [4].

TABLE 1

COMMON DSSC DYES AND THEIR CHARACTERISTICS [4].

Sensitizers	k_{inj} [s^{-1}]	[V] [cm^{-1}]	t_f [ns]	Quantum yield
$Ru^{II}(bpy)_3$	2×10^5	0.04	600	0.1
$Ru^{II}L_3$ (H_2O)	3×10^7	0.3	600	0.6
Eosin-Y	9×10^8	2	1	0.4
$Ru^{II}L_3$ (EtOH)	4×10^{12}	90	600	1
Coumarin-343	5×10^{12}	100	10	1
$Ru^{II}L_2(NCS)_2$	10^{13}	130	50	1
Ti_S^{IV}-Alizarin	$>10^{13}$	5×10^3	-	1

NOTE: "In the sensitizers column, L stands for the 4,4‟-dicarboxy-2,2‟bipyridyl ligand and bipy for 2,2‟-bipryidyl."[4]

The electron injection coefficient (k_{inj}), the electronic coupling matrix element (|V|), the excited state lifetime (t_f), and the quantum yield of the dyes are compared. The term k_{inj} represents the rate at which electrons are transferred from the dye to the semiconductor, so that the larger the term, the faster electrons can flow through in the cell [4]. The variable |V| estimates the degree of change between the initial and final wave functions of the electron moving between the dye and the semiconductor. This value may be used to calculate k_{inj} via equation (1.8), which is called the Fermi Golden Rule [29]. In this equation, h stands for Planck‟s constant and ρ represents the density of the holes in the semiconductor‟s conduction band [4].

$$k_{inj} = \left(\frac{2\pi}{h}\right)|V|^2\rho \tag{1.8}$$

The quantity t_f in Table 1 is the length of time between absorption of a photon by a dye molecule and the emission of energy that returns the dye molecule to its ground state. The quantum yield of a dye is the ratio of the number of electrons it emits to the number of photons it absorbs [30]. The numeral "1" given for the last four dyes in the table represents near-perfect conversion. The dye $Ru^{II}L_2(NCS)_2$ (long form *cis*-dithiocyanato-bis(2,2'-bipyridyl-4,4'-dicarboxylate)-ruthenium(II)), also known as N3 dye, has garnered a high volume of study because of its ability to bind to TiO_2 and its electron transfer characteristics. Figure 14 shows the attachment of an N3 dye molecule to the surface of TiO_2. The separation is in angstroms. Another variety of dye popular in studies is "black dye", so called because of its color, has the chemical formula Ru(4,4',4"-tricarboxy-2,2':6,2"-terpyridine)$(SCN)_3$ [10, 24]. These two dyes have high IPCEs across a wide range of light wavelengths, as shown by the graph in Figure 15 [10].

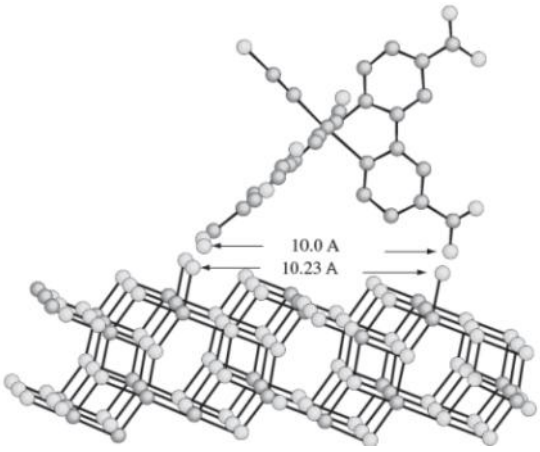

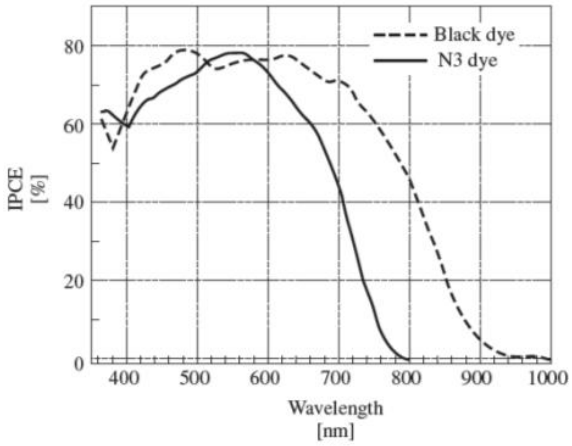

Figure 14 (left): Attachment of dye molecule to TiO_2 substrate by carboxyl groups [10].
Figure 15 (right): IPCE vs. light wavelength for N3 dye and black dye [10].

The dyes described above are synthetic compounds that can be expensive to produce. The purchase price of black dye, mentioned above, can be $3 to $5 per milligram. The price of N3 dye can fall to $0.55 per milligram if it is purchased in bulk [31]. In addition, those

chemicals based on ruthenium can be toxic when oxidized [31, 32]. With this in mind, researchers continue to search for alternative sensitizers. One group of dyes that continue to be investigated are the anthocyanins. Like chlorophyll, these are natural organic dyes derived from plant matter, in particular, dark blue, red, or purple fruits like blackberries and raspberries. DSSCs made using blackberry juice are sometimes referred to as "blackberry cells." In addition to being inexpensive and readily available, these dyes have a very rapid conversion rate; cyanin, a member of this dye family, has an injection coefficient in the range of 10^{13} s^{-1}. Its excited state lifetime has been estimated at less than 100 fs. However, the dyes are slow to recharge from the surrounding electrolyte. At present, this limits their efficiency. Anthocyanin dyes also have a wide absorption spectrum, reaching from the red end of the spectrum into the ultraviolet [33].

A final concern with regard to dye selection is the lifetime of the molecules themselves. The continuous absorption and release of energy can break down the molecules, causing a cell to lose efficiency over time. Some of the damage to dye molecules may also be due to UV exposure. It has been found that the addition of a transparent UV filter to the front glass covering of a cell increases the lifetime of the cell [33]. Because most dyes absorb photons below the ultraviolet light range, this does not substantially reduce the energy generation potential of the cell.

2.3.3 Electrolyte

While bromine, hydroquinone, and other redox electrolytes have been employed in DSSCs, the most successful cells have been made using iodine based electrolytes [10]. For DSSCs that require a less reactive substance, the alternatives have been a cobalt(II/III) based redox reaction or a Na_2S electrolyte, but neither of these substance yields a cell with an efficiency that equals that of iodine based cells [34]. At the counter-electrode, a negatively

charged triiodide molecule takes on two electrons and is transformed into three separate iodide atoms, as shown in the reaction in equation (1.9):

$$I_3^- + 2e^- \leftrightarrow 3I^- \quad (1.9)$$

The reaction is reversed when the iodide atoms contact the electron deficient dye, which acquires two electrons from the electrolyte, causing the triiodide molecule to reform [4, 10]. There is a potential for the semiconductor film to transfer electrons to the electrolyte instead of directing the current out of the cell; this is called dark current [4, 10, 24]. To combat this tendency, chemicals such as tert-butylpyridine (TBP) are sometimes added to the cell to fill in any vacancies left by the dye [10].

2.3.4 Electrodes

TCO glass is used as the substrate for the semiconductor and for the counter-electrode. This consists of plate glass with a coating of a clear semiconducting material, such as fluorine-doped SnO_2 or indium tin oxide (ITO). The glass may also be platinized to improve its effectiveness as a conductor [10]. This replaces standard counter-electrodes that consist of a sheet of glass covered in thin wires that obstruct 3% to 5% of the surface area of a cell. TCO glass is especially useful in cells that contain materials with a high electrical resistance, and require the maximum possible surface area to be in contact with the electrode [35]. While it is important that the photo-electrode be transparent, it can be advantageous to have a counter-electrode substrate that reflects or refracts light. A ray of light entering a DSSC and can impact rough surfaces and be scattered throughout the cell. Any light that passes through the dye without being absorbed does not contribute to current production. However, if the light is reflected back into the dye, the dye has a second opportunity to absorb its energy [24].

2.3.5 Manufacturing Methods

The most important advantages of DSSCs over conventional cells are the ease of manufacture and the reduced cost. The procedure for creating a monocrystalline silicon cell requires considerable time and expense. First, the silicon must be extracted from quartz, a silicon dioxide crystal. Then it must be purified to remove any particles that could create dislocations within the lattice of the silicon. Next, the silicon must be melted at around 1400 °C and then cooled very slowly into a cylindrical structure with large crystals and a minimum of grain boundaries. Once cooled, the silicon is sliced into wafers using a wet wire saw; this sacrifices a considerable amount of silicon material between wafers. Because silicon is very brittle, a minimum film thickness of around 300 μm is needed. Finally, the silicon must be etched and doped with phosphorous and boron. This wafer-type, multi-crystalline solar cell is sometimes referred to as a first generation photovoltaic device [1].

Second generation devices are typically thin film solar cells. It should be noted that this type of photovoltaic is less efficient than a first generation cell, but is more cost effective. Thin film cells can be up to one hundred times thinner than first generation devices, which considerably lowers their expense. Their lower manufacturing temperature, between 200 and 500 °C, is also a cost saver. These cells are often created through the chemical vapor deposition of semiconductors onto a substrate such as TCO glass. Other manufacturing methods include co-evaporation, spray pyrolysis, and electrodeposition. Films can be constructed from amorphous silicon, $Cu(InGa)Se_2$, and cadmium telluride [1].

The construction of a DSSC begins with the creation of the photo-electrode. As an example, instructions for the manufacture of a TiO_2 cell are summarized here. Nanoparticles of TiO_2 can be obtained commercially, or they can be manufactured by the method. The chemicals

used and the length of the heat treatment can be adjusted to create particles of varying sizes. If the particles are treated above 240 °C, the nanoparticles will tend to contain rutile instead of anatase. Also, if the particles are not treated above 230 °C, they will tend to make a clear electrode film; otherwise the film will likely be opaque [10]. Usually, TiO_2 particles are deposited on a sheet of platinized TCO glass using one of two methods: doctor blading or screen printing [4, 10]. Doctor blading involves mixing a solution of TiO_2 and spreading it evenly over the surface of the glass. This method as it applies to this project is discussed in detail in Section 3.3.2.2. Screen printing requires a similar paste composed of TiO_2, polymers, and ethanol. A film is then layered onto the substrate using a screen printer [10].

Both processes should use approximately 1-2 mg of TiO_2 per square centimeter [10]. Care should be taken to apply a very thin layer of the semiconductor because too thick a film can create an obstacle to electron flow. The thickness of the film should be no greater than the diffusion length, L_D, of the electrons. The formula for this length is given by equation (1.10).

$$L_D = (D\tau)^{1/2} \tag{1.10}$$

The variable D represents the diffusion coefficient of the nanocrystalline material, and τ stand for the average recombination time of an electron time traveling through the material. Both of these values are determined experimentally [17]. On the other hand, if the semiconductor film is too thin, there may be insufficient material present to capture and extract a maximum amount of energy from light.

At this point, both types of film need to be sintered. The nanoparticles that compose the film are disconnected, and so it is difficult for current to pass through the film. Sintering at several hundred degrees Celsius causes necking between the particles. These thin connections allow the semiconductor to transfer current [36]. The heating also removes the solvents and

fillers used in the construction of the films. The sintering temperature can have an important effect on the current generated by the cell, as shown in Figure 16. A low sintering temperature, around 350 °C, creates less necking than a film sintered at 550 °C, so the conductivity of the first film is lower. However, as sintering temperature increases, surface area of the film decreases, so that dye cannot be absorbed as deeply into the film. If too much surface area is consumed, the cell will lose efficacy [37]. Most films are sintered between 450 and 500 °C [10].

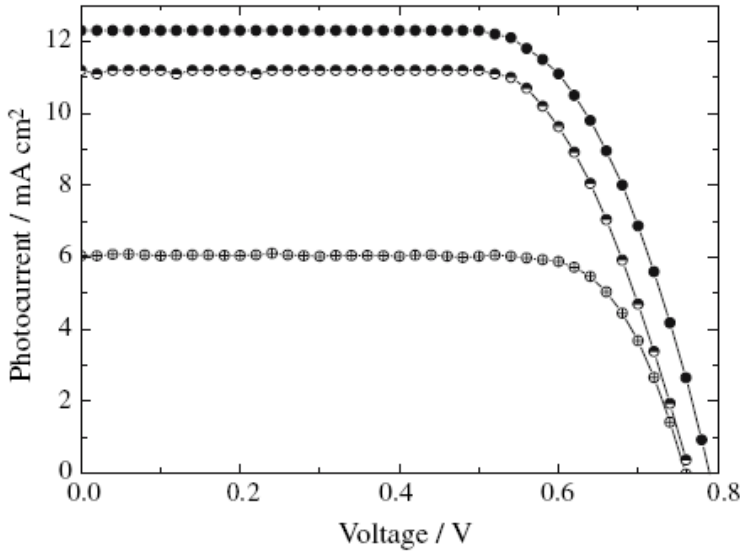

Figure 16: Current vs. voltage based on identical TiO_2 samples sintered at 350 (lowest curve), 450 (middle curve), and 550 °C (top curve) [37].

After sintering, dye and the electrolyte are applied to the film. Dye can be applied by drops or by immersion of the film for between 12 and 24 hours [10, 38]. Some procedures call for either the film or the dye to be heated before application to improve dye absorption [39]. In one experiment, the photo-electrode was boiled in the dye [40]. After the dye has been applied, the film can be cleaned with ethanol to remove excess dye molecules (as mentioned previously, excess dye impedes light absorption) [41]. The electrolyte, typically iodine based, is next applied to the cell. Finally, the counter electrode is placed on top of the cell and the edges may be sealed to prevent leakage of the dye and electrolyte [10]. The seal may take various forms;

one example would be a hot-melt ring of a specific thickness [42, 43]. A UV filter, such as A 50 μm thick polyester film, may or may not be added to the top of the photo-electrode [44].

In addition to the cost and manufacture of the solar cell portion of a photovoltaic device, there is an additional expense associated with what is referred to as the "balance of the system" (BOS). This includes the support structure for the cells and the wiring required to integrate them into a grid. It may also cover motors used to rotate the cells to optimize the incident angle of the sunlight that strikes them. And, because most solar panels consist of several solar cell segments, a frame is required to hold the cells. In some cases, these secondary photovoltaic components can be almost as expensive as the cells themselves [1]. Figure 17 shows a bar chart estimating the time required for a first or second generation photovoltaic cell to pay for itself at the present time and the payback time anticipated in the future. The figure considers the solar cell itself and the BOS [24]. DSSCs fall into the third generation of solar cells. As with second generation cells, third generation devices do not yet match the efficiency of the first generation, but their low cost makes them competitive. The estimated payback time for a DSSC and its BOS at this time is three to five months [24].

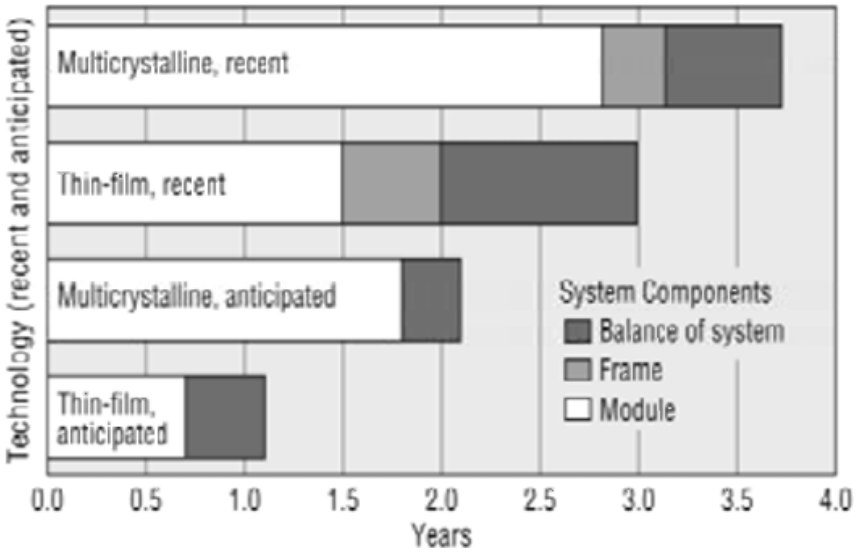

Figure 17: Anticipated payback time for various types of solar cells [24].

2.3.6 Practicality

A fundamental question that should be asked in the evaluation of any new technology is whether or not it is practical. The cost and availability of the resources required to create the item should be considered, as well as the existing technologies with which the new device is likely to compete. In the case of DSSCs, there are a surprising number of competitors, including other alternative energy technologies, such as wind and nuclear, as well as conventional solar cells. A study published by the American Chemical Society compiled expert evaluations of the future of photovoltaic technologies and it lists twenty-six different varieties of photovoltaic cell. Table 2 summarizes the main varieties of solar cells that are either in production or being researched around the world. DSSCs are listed under the „excitonic" variety of cell as 4c [45].

TABLE 2

PHOTOVOLTAIC CELLS UNDER INVESTIGATION [45].

major category	subcategory	major category	subcategory
1. crystalline-Si	1a. c-Si	4. excitonic	4a. organic, small molecule
	1b. mc-Si, wafer-based		4b. organic, polymer
	1c. mc-Si, ribbon or sheet		4c. dye-sensitized TiO_2
	1d. mc-Si, novel		4d. hybrid organic/inorganic
2. thin-film	2a. a-Si/multijunction a-Si		4e. quantum dot composite
	2b. thin Si	5. novel, high-efficiency	5a. hot carrier
	2c. CdTe		5b. multiple electron–hole pair
	2d. CIS and related alloys		5c. multiband
	2e. polycrystalline multijunction		5d. frequency up/down conversion
	2f. novel materials		5e. plasmonics
3. concentrator	3a. c-Si, up to 100×		5f. thermophotovoltaics
	3b. c-Si, 100–1000×		
	3c. III–V multijunction, up to 100×		
	3d. III–V multijunction, 100–1000×		
	3e. novel		

The authors of the study described above estimate that for photovoltaics to compete effectively with other energy sources on a large scale, the energy created by the cells must cost \$0.30 per peak watt (W_P). At present, solar energy from first generation cells costs about \$4.50 per W_P if the BOS is discounted and almost \$9 per W_P if the BOS is included. Energy produced by other alternative technologies range from \$1.60 per W_P for wind to \$4.00 W_P for nuclear

power. The estimates do not take into account capacity factors, which are a way of accounting for the average energy that a technology produces over time. In the case of wind energy, a 0.4 capacity factor accounts for variable wind speeds or for a lack of wind. For photovoltaics, a 0.2 capacity factor compensates for overcast days when little energy is produced and for night. These two scenarios contrast with the 0.9 capacity factor for nuclear energy; nuclear power plants can be operated almost continuously without regard to environmental effects. If these capacity factors are considered, the price of photovoltaic energy jumps to at least $25 per W, wind becomes $4 per W, and nuclear climbs to $4.40 per W. This shows the significance of the gap between the present cell performance and that which may be required in the future [45].

In order to improve their chances of competing against conventional solar cells, DSSCs require lower material and manufacturing costs, and/or higher efficiencies. The former have been achieved to some extent for liquid DSSCs. The typical DSSC semiconductor material, TiO_2, is one of the fifty most common substances used in industry and does not require the level of refining necessitated by silicon [1]. Also, less semiconductor material is required in DSSCs, which are much thinner than silicon cells [10]. TCO glass is more expensive than standard electrical contact glass, but this cost is canceled by the increased efficiency it promotes in DSSCs [35]. Iodine is once again a common and inexpensive material, but necessary additives that maximize electrolyte performance drive up the price. As previously mentioned the cost of dyes can be high if they are artificial. One gram of N3 dye, if purchased in bulk, costs between $240 and $550 [31, 32]. The price of anthocyanin dyes is much lower, and depends entirely on the price of the fruit from which they are derived [33]. Though DSSCs require a greater number of components than silicon cells, they can be made at lower temperatures and with less effort than is required to refine silicon [1, 36].

DSSC efficiency is highly variable depending on the components and manufacturing method employed. At present, the record efficiency achieved by any photovoltaic cell is 41.1%, a benchmark set by the Fraunhofer Institute of Solar Energy Systems (ISE) in Germany with a GaInP/GaInAs cell in 2009 [15]. This is an exotic cell, and not typical of most photovoltaics currently manufactured. High efficiency silicon cells have reached 20 to 25% efficiency, though commercial cells tend to have efficiencies in the teens. The average efficiency required for a solar cell to be considered viable is around 10% [1]. DSSC efficiencies have been reported that exceed the 10% barrier [14, 38, 46], but most liquid cells have efficiencies between 4 and 8%. For quasi-solid state and solid state cells, the efficiency rarely climbs to 4%. Future breakthroughs may allow the average efficiency to rise higher.

Another consideration with regard to a cell‟s usefulness is lifetime, and the lifetime of a DSSC is shorter than that of a conventional cell. It is estimated that a silicon cell remains useful for thirty years, but cells can last longer. At present, the best DSSCs have only a ten year lifespan. It should be noted that however long a cell‟s rated lifetime, cell efficiency drops continuously. This is true of first, second, and third generation cells. The lifespan and efficiency of DSSCs may be improved by new advances in quasi-solid state and solid state technology. It is also possible that maintenance cycles that replace exhausted components, such electrolytes, could extend DSSC usefulness. Whether or not this would be cost effective is unknown [45].

Because DSSCs are a new product, there is not a commercial testing standard for them. It may be assumed that the testing standards that will be applied to them will be similar to those that are applied to first generation cells. If this is so, DSSCs sold commercially may be evaluated as follows: exposure to ultraviolet light at between 55 and 60 °C for 1000 hours, an accelerated thermal test at 85 °C for 1000 hours, and humidity and temperature trials [24].

CHAPTER 3

RESEARCH APPROACHES

3.1 Basis of Procedure

The processes employed in this research are modeled on a paper published in 2008 by Ito et. al. which produces high efficiency DSSCs. The paper details the production of a multi-layered DSSC with light absorbing and light scattering layers made by screen printing. The quantity of material in each batch produced using this method is high, with 16 g of TiO_2 used per batch [38]. In order to manufacture and test a variety of TiO_2 pastes of different composition economically, it was necessary to scale down this procedure and adapt it to more common laboratory equipment. All the same chemical components are employed, with the exception of titanium tetrachloride. The Ito et. al. paper employs two titanium tetrachloride surface treatments in the production of the photo-electrode as a means of reducing contamination and improving the surface characteristics of the semiconductor films. It can lead to a 10% improvement in cell performance [38]. Due to constraints outlined in Section 3.6, a 0.1 M HCl bath, also mentioned by the Ito paper [38], was substituted. Also omitted was the hot melt spacer used to separate the electrodes.

3.2 Semiconductors

A variety of materials have been used for DSSC semiconductor electrodes. As stated previously, the most common and most effective is TiO_2, which is the primary material selected for this project. In order to test the effectiveness of the layering techniques, an additional material was included in some layers. This deliberate addition alters the properties of the TiO_2 based films to a measurable degree and in a way that should be predictable. In this case, graphene was selected as an additive material.

3.2.1 Graphene

Some of the more important nanomaterials that have been investigated in recent years are fullerenes. These are composed of carbon atoms that are often arranged in a hexagonal structure in which each atom is bonded to three others. Graphene, shown in Figure 18, is a two dimensional sheet of carbon atoms arranged in this fullerene pattern. For graphene, each carbon bond is 0.142 nm in length [47]. Because carbon has four valence atoms but only forms three bonds in a hexagonal structure, the fourth electron is "distributed" across these three bonds, making them stronger than a single bond. It can also contribute to increased conductivity in nanomaterials with this atomic lattice [48].

Graphene is known to be more conductive than TiO_2, therefore pastes containing graphene should be more conductive and exhibit a greater current than unmodified pastes [48]. However, after a point additional graphene could become detrimental to cell performance by blocking light access to the interior of the semiconductor film. Graphene has previously been used to improve the performance of DSSCs. Yang et. al. found that TiO_2 doped with 0.6 wt % graphene showed an improved short circuit current and efficiency compared with undoped TiO_2. They also tested TiO_2 doped with 2.5 wt % and higher graphene, and found performance severely inhibited [49]. The threshold at which graphene begins to inhibit performance has not been pinpointed.

Graphene sheets layered in bulk form graphite [47, 48]. On a smaller scale, graphene sheets can also form nanoflakes like those used in this research. The graphene nanoflakes employed herein were acquired from Angstron Materials, and were rated to be no more than 10 nm thick. A container of graphene is pictured in Figure 19.

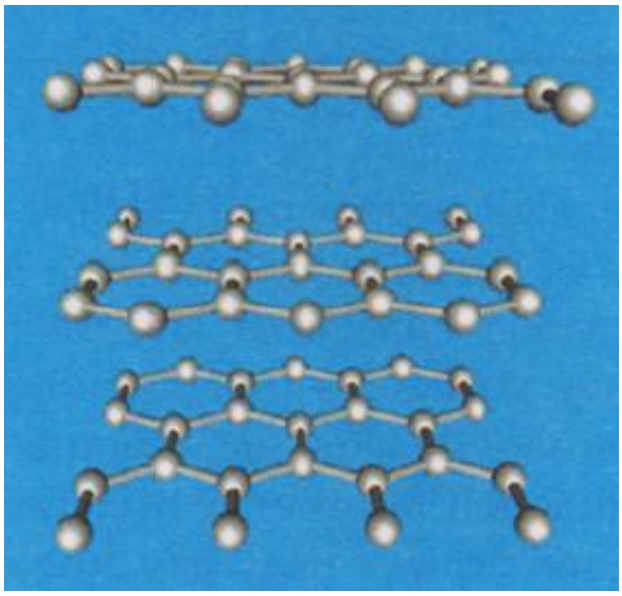

Figure 18: (left) Sample graphene sheets composed of interlocking carbon atoms [47].
Figure 19: Graphene purchased from Angstron Materials.

3.2.2 Manufacture of TiO_2 Nanoparticle Pastes

A vast number of procedures for creating TiO_2 pastes exist. The process employed in this research is modeled on a paper published in 2008 by Ito et. al.[38] The quantities were scaled down and the steps have been modified based on equipment and chemical availability. All chemicals were acquired from Sigma Aldrich unless otherwise specified. The basic formula for each paste included: 2 mL of ethanol, 1.63 g of terpineol, 1.125 g of a 10 wt.% ethyl cellulose (5-15 mPas) in ethanol solution, 0.875 g of a second 10 wt.% ethyl cellulose (30-50 mPas) in ethanol solution, and a quantity of semiconductor material. The mass of semiconductor used, and the combination of materials in the semiconductor, are listed in Table 3.

As Table 3 shows, two plain TiO_2 samples and five TiO_2 samples mixed with the additive – graphene – were tested. Within the pair of plain TiO_2 samples, the paste containing 25 nm diameter anatase nanoparticles was intended to serve as the primary light absorbing layer. The 100 nm diameter anatase and rutile nanoparticle based paste was meant to act as a light scattering

layer. All graphene containing pastes had 25 nm diameter TiO_2 as their primary semiconductor. Quantities were measured with care using an enclosed Ohaus Adventurer SL scale.

TABLE 3

SEMICONDUCTOR PASTE COMPOSITIONS TESTED.

Total Mass (g)	Base Semiconductor	Mass of Base Semiconductor (g)	Additive Material	Mass of Additive Material (g)	wt.% of Additive Material in Semiconductor
0.4230	TiO_2 (25 nm)	0.4230	-	-	-
0.8450	TiO_2 (100 nm)	0.8450	-	-	-
0.4230	TiO_2 (25 nm)	0.4222	Graphene	0.0008	0.20
0.4230	TiO_2 (25 nm)	0.4213	Graphene	0.0017	0.40
0.4230	TiO_2 (25 nm)	0.4205	Graphene	0.0025	0.60
0.4230	TiO_2 (25 nm)	0.4196	Graphene	0.0034	0.80
0.4230	TiO_2 (25 nm)	0.4188	Graphene	0.0042	1.00

Each of the seven semiconductor combinations listed in Table 3 was combined with the other precursor chemicals listed above in a small glass vial. In order to achieve a uniform consistency in the final product, 15 small glass seed beads, rinsed in ethanol and then dried, were added to each vial. During mixing, these beads break up larger nanomaterials clumps that are otherwise difficult to disperse. Mixing began when the vial was placed on a pulsing vortex mixer (Fisher Scientific, set to 3000 rpm), as shown in Figure 20, for 1 to 2 minutes. It was then moved to a sonicator (Fisher Scientific), which is pictured in Figure 21, for 30 minutes. A second 1 to 2 minute round on the pulsing vortex mixer followed, then a second 30 minute session in the sonicator. After mixing a final time on the pulsing vortex mixer, the fluid inside the vial was smooth, with no visible aggregations.

Figure 20: (left) Glass vial on pulsing vortex mixer.
Figure 21: Sonicator used for further mixing.

Once the solution was thoroughly mixed, it was immediately transferred to a crucible on a hotplate. The solution was heated to approximately 60 degrees (which was below its boiling point) to facilitate evaporation of the ethanol. Every few minutes the solution inside the crucibles was shaken to insure even evaporation. Progress was assessed by tipping the crucible and observing the flow of the paste along the side of the crucible. When the paste had thickened significantly, and adhered to the surface of the crucible when tilted, it was considered finished. A material spatula dipped into the paste and then pulled out left a visible peak that did not immediately sink. The paste was then transferred to a plastic container for storage; tape was used to seal the container to make sure the paste did not dry further.

3.3 Electrode Production

The creation of the photo- and counter-electrodes required slides of ITO coated glass measuring 1 in. x 1 in. The slides were cut in fourths by scoring with a glass cutter and breaking

by hand. Half of the resulting pieces, each roughly 0.5 in. x 0.5 in., were used for photo-electrodes. The second half of the glass pieces were employed as counter-electrode substrates.

3.3.1 Cleaning of Glass Slides

The glass pieces used for both electrodes required extensive cleaning. First, each substrate was washed with dishwashing liquid soap and rinsed thoroughly with water. The glass was then placed in a beaker containing a 0.1 M solution of HCl at 70 °C for 30 minutes. Next, the slides were removed from the acid solution and rinsed with ethanol. An oxygen plasma treatment followed. Each piece was placed conductive-side up on a small glass plate, which was then set inside the oxygen plasma chamber. The vacuum connected to the chamber was turned on, the chamber lid was put in place, and the plasma was activated. The glass was treated for three minutes on a medium setting. The plasma flow was monitored during this period and adjusted to a maximum level when necessary.

3.3.2 Photo-electrodes

Photo-electrodes were prepared using three methods – screen printing, doctor-blading, and stamping – to apply the nanoparticle pastes created in Section 3.2.2.

3.3.2.1 Screen Printing

As a basis of comparison with layered cells created by alternative means, TiO_2 photo-electrodes were created by screen printing with 25 nm TiO_2 paste and then tested with N-719 dye. The results of these tests are summarized in Section 4.1. A small Speedball commercial screen printing kit was purchased, and masking tape was used to create the shape and size of the semiconductor film on the screen. Films composed of five, ten, and fifteen layers were tested to see which provided the best efficiency for subsequent comparisons.

3.3.2.2 Doctor Blading

Single layer test versions of each paste were made by standard doctor-blading for initial testing. Thin pieces of tape were cut and overlapped on the surface of the glass to form a rectangular channel. For layered doctor-bladed films, pieces of tape were cut from a Scotch tape roll and a hole was made in each piece using a 0.1875 in. (0.4763 cm) diameter punch. The use of holes insured that the height of the tape above the glass was uniform. In each case, tape was placed on the conductive side of the photo-electrode glass, with the void positioned entirely on the glass. Paste was deposited on the coated glass slide at one end of the tape, and then spread evenly over the surface of the glass using a clean glass stirring rod. The tape was removed, and the glass slide was transferred to a hot plate set to 125 °C for six minutes. To make additional layers, the slides were re-taped by lining up the punched holes in the subsequent pieces of tape with the first layer on the glass. Paste was applied with the stirring rod, and the 125 °C heat treatment was repeated between layers. Several slides were usually prepared at one time; slides on a hotplate are shown in Figure 24. The single layer film results are discussed in Section 4.2 and the multi-layer film results are discussed in Section 4.4.

3.3.2.3 Stamping Method

The creation of stamped photo-electrode films involved latex-free porous cosmetic foam sponges like those in Figure 22. In theory, the porous surfaces of the foam, shown magnified in Figure 23, creates a similar texture to that achieved by screen printing. Though the polymers present in the original paste contribute to a high degree of film porosity, a textured applicator may contribute even further. As increased porosity leads to increased dye uptake and light penetration, this could significantly impact cell efficiency.

The foam was cut to size, and then rinsed in ethanol to remove any impurities. The stamps were then allowed to dry thoroughly. Paste was applied to the foam using a clean glass stirring rod. No excess paste should be visible on the surface of the stamp so that the material distribution in the layer will be uniform. Also, the stamp should not be permitted to become too dry, as it could adhere to the surface of the existing film instead of depositing additional layers. The glass was stamped in one stroke and blotted with the same piece of foam in a second stroke. Blotting serves to further distribute the paste, remove excess, and to even the surface. The layers in a stamped film do not settle appreciably. After each layer was formed, the photo-electrode was moved to a hot plate at 125 °C for six minutes to set the paste.

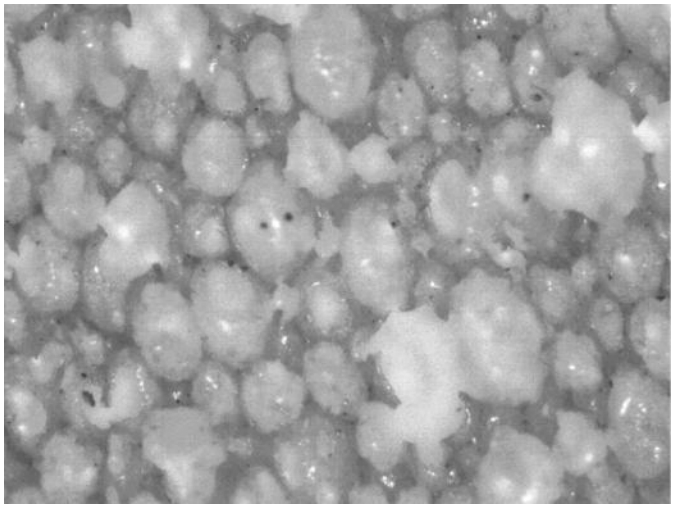

Figure 22: (left) Foam sponge employed in stamping method.
Figure 23: Surface of foam magnified five times by an optical microscope.

In instances where different pastes were employed for different layers of the same cell, a separate stamp was used for each paste. The testing results for multi-layer stamped cells appear in Section 4.5.

3.3.2.4 Heat Treatment

At this point, a stepped heat treatment procedure was followed based on the paper by Ito et. al. After six minutes at 125 °C, the hot plate was set to the following temperatures and held

there for the lengths of time given: 325 °C for five minutes, 375 °C for five minutes, 450 °C for fifteen minutes, and 500 °C for fifteen minutes [38]. Heat treatment at these high temperatures initiates a process called sintering, in which the nanoparticles begin to melt and form narrow bridges between one another other that allow electricity to be conducted across the film. Beginning around 325 °C, the TiO_2 films undergo a color change, as shown in Figure 25. This occurs regardless of any added doping material, and the films turn white again as they climb to higher temperatures. After heat treating to 500 °C, the glass slides' temperature was stepped down by 45-75 °C every thirty minutes until the slide reached 80 °C. This slow cooling prevented both the glass substrate and the film from cracking as they cooled. Completed films are shown in Chapter 4.

Figure 24: Hotplate used for heat treating photo- and counter-electrodes.

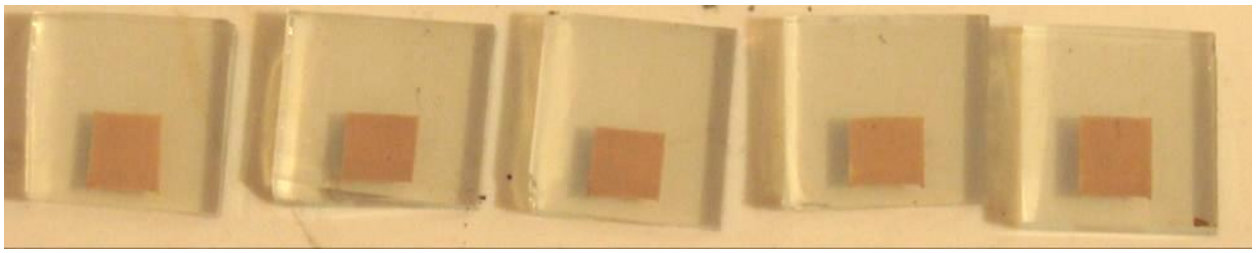

Figure 25: TiO_2 based cells undergoing a color change during heat treatment.

3.3.3 Counter-electrodes

The glass pieces for the counter-electrodes underwent an additional purification step after removal from the oxygen plasma chamber. To remove organic contaminants, the glass was heated to 450 °C for 15 min. It was then cooled to room temperature. Meanwhile, a chloroplatinic acid solution was formed by adding 2 mg of H_2PtCl_6 powder to 1 mL of ethanol. A drop of the solution was placed on the conductive surface of each of the counter-electrodes. They were then heat treated to 400 °C for 15 min. Counter-electrodes were reusable from solar cell to solar cell, but were carefully cleaned with ethanol between each use. After their use in three or four cells, the glass was re-platinized using the procedure above.

3.4 Dye

Standard N-719 and N-3 dyes were used in these experiments. A 0.2 mM N-3 dye solution was created by adding dye powder to ethanol. Both the dye powder and solution were a dark purple. Dyeing began immediately following photo-electrode heat treatment, when the glass was at 80 °C. Each photo-electrode was submerged in the dye for 22 hours. It was then removed and excess dye was rinsed off with ethanol. It then dried in air for 24 hours prior to testing. Images of dyed films appear in Chapter 4.

3.5 Assembly of Cells

After the 24 hour drying period needed by the photo-electrodes, assembly began. To insure that only a known area of the semi-conductor film was tested, a mask was placed on the

exterior, non-conductive surface of the photo-electrode. The mask consisted of a light blocking material with a 0.00000794 m^2 area window in it. The mask was adhered to the exterior of the glass using a very small quantity of Elmer‟s glue. Next, the photo-electrode was carefully lowered conductive side down onto the counter-electrode. Once the electrodes were in position, small binder clips were used to hold them together.

The last step in assembly was the addition of the electrolyte. In this case, the electrolyte described by Ito et. al. was employed. In consisted of 8.5 mL of acetonitrile, 1.5 mL of valeronitrile, 1.597 g of 1-butyl-3-methyl imidazolium iodide (BMII), 0.076 g of iodine, 0.118 g of guanidine thiocyanate, and 0.676 g of 4-tert-butylpyridine [38]. One drop of fluid was deposited on the seam between the glass pieces. Capillary action pulled the liquid into the interior of the cell. This was aided if necessary by gently opening and closing the binder clips that held the glass together. Final assembly of the cells was performed the day of the testing in each case.

3.6 Safety

A final concern regarding DSSC manufacturing is toxicity. Conventional silicon cells are largely inert once completed, though during production care must be taken to minimize worker exposure to silica dust, which can cause lung disease. Because DSSCs contain a number of components, there are more materials to be examined. The components most likely to cause concerns are the liquids. As previously mentioned, some of the most common dyes used in DSSCs are based on the rare metal ruthenium, and are irritants if ingested or breathed. If they are oxidized, they can become toxic [32]. Organic dyes, such as the anthocyanins, are non-toxic, but have not yet yielded the same results as inorganic dyes [33].

Several of the chemicals employed in the electrolyte are potentially harmful. Iodine is a normal compound used by the human body. The recommended daily value of iodine is around 0.17 mg. Long-term excess iodine ingestion is known to cause thyroid complications and increase the incidence of goiters. However, these consequences are most often noted in individuals who have consumed iodine consistently, such as when it acts as a water purifier. None the less, iodine should be handled with care [50]. Other electrolyte chemicals, such as acetonitrile, valeronitrile, and 4-tert-butylpyridine are highly flammable, even in vapor form [51-53]. Most of the chemicals in the electrolyte – including acetonitrile, valeronitrile, 4-tert-butylpyridine, terpineol, and BMII – can cause eye, lung and skin irritation [51-55]. For this reason, all operations involving the electrolyte solution should be conducted in a fume hood.

The most common semiconductor material in DSSCs is TiO_2. Numerous studies have been conducted on the potential health risks associated with TiO_2 over the past forty years because of its extensive use in products such as paint, foods, sunscreen, and make-up. The National Institute for Occupational Safety and Health (NIOSH) has stated concerns about the inhalation of TiO_2 at concentrations of 5000 mg/m^3 or higher because testing with rats has shown a slight increase in lung fibrosis from continual exposure. However, rats are highly sensitive to inhaled particulates, so the potential impact on humans is uncertain. It is best that TiO_2 powders be used in a fume hood for safety. Ingestion testing found that no TiO_2 traveled outside the digestive tract in rats, dogs, guinea pigs, rabbits, cats, or humans, and that TiO_2 caused no adverse effects when consumed. Skin exposure to TiO_2 may be a more significant concern. Studies suggest that while TiO_2 produced by typical manufacturing methods is not absorbed by the skin, nanoparticles of the material can be absorbed by skin cells. Particles less than 50 nm in diameter easily pass into skin cells, and at less than 30 nm they can enter nerves. If skin cells

containing TiO_2 are then exposed to sunlight, a harmful photocatalytic reaction can occur that may damage DNA in the cells. Skin exposure to TiO_2 particles on a micro- or nano-scale should be avoided [56].

Graphene, as mentioned above, falls into the fullerene category of nanomaterials. The most studied materials in this category are carbon nanotubes, and the impact of graphene on the human body would likely be similar. Carbon nanotubes have been shown to cause granulomas in the lungs of mice at much lower levels of exposure than carbon black. One study suggested that three weeks of exposure to concentrations of 5 mg/m^3 could cause lung lesions. All operations involving graphene should be performed in a fume hood, or should be conducted by personnel equipped with respirators and goggles [57].

Two other hazardous chemicals that are used in the Ito et. al. paper are chloroplatinic acid and titanium tetrachloride. Chloroplatinic acid is toxic if ingested, and can trigger asthmatic breathing and damage to the upper respiratory tract if inhaled. It is corrosive, causing severe skin burns on contact. It should never be used without proper skin protection (gloves and aprons) or outside a fume hood [58]. Titanium tetrachloride on the other hand cannot be safely used in a standard fume hood. It is a liquid that reacts violently with water, so much so that it cannot be opened in an air atmosphere because it reacts with water vapor. The fumes it releases are poisonous. This material should be used in a glove box in an argon or nitrogen atmosphere. It is also corrosive [59]. Of the chemicals mentioned thus far in connection with DSSCs, titanium tetrachloride is the most difficult to work with, and the most dangerous, which makes it the least practical for use with common, basic lab equipment. Therefore, the titanium tetrachloride treatments discussed in the Ito paper, thought they are credited with doubling efficiencies in some cases, are foregone in these experiments [38].

3.7 Testing

The DSSCs created in the course of these experiments were tested with a solar simulator. This consisted of a Xe lamp in a Newport Research Arc Lamp Housing, Model 67005. A solar simulator projects light of known intensity and wavelengths, in this case AM 1.5, onto a solar cell. Alligator clips are used to attach the photo-electrode and counter-electrode of the cell to a monitor that registers current and voltage at low levels. This monitor transmits data to a computer where it is recorded in text files. Images of the solar simulator components appear in Figure 26. Several tests were run on each functional solar cell; of special importance was the determination of the current vs. voltage curve. Film surface characteristics were assessed using an atomic force microscope (AFM).

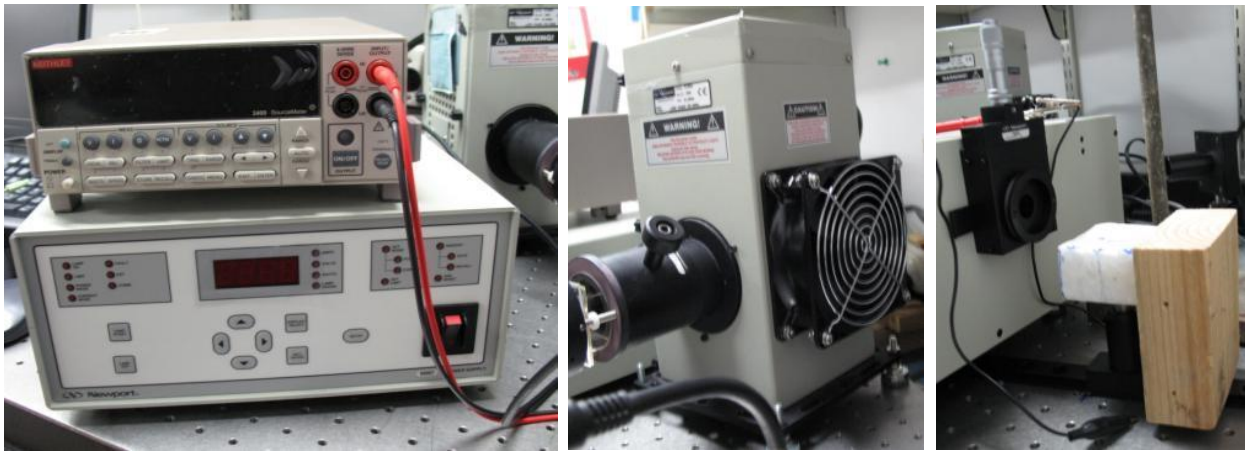

Figure 26: Images of a solar simulator arrangement.

CHAPTER 4

RESULTS & ANALYSIS

4.1 Screen Printing

The screen printed films developed an uneven surface texture that made it difficult to determine an average film thickness. The surface of a fifteen layer cell is visible in Figure 27. The contrast on the image has been increased to make the texture more visible.

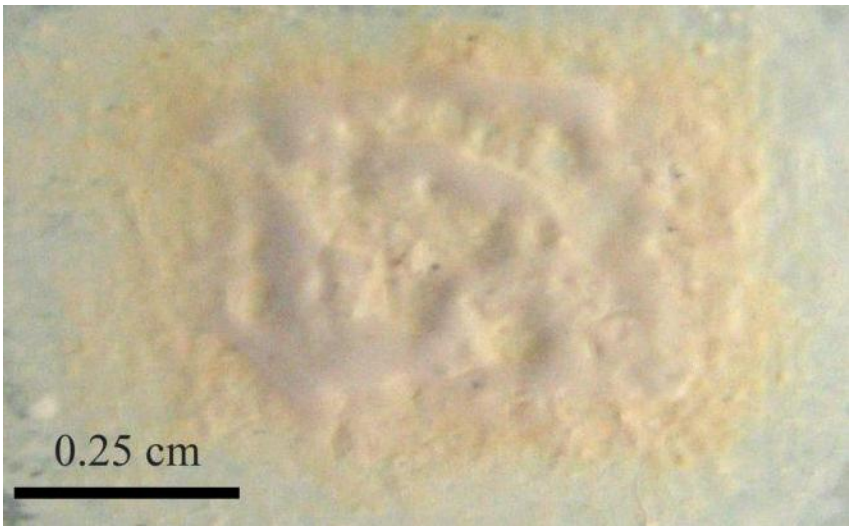

Figure 27: Surface of screen printed film.

This degree of irregularity and the unusual thickness of the fifteen layer cell made it unsuitable for testing. The five layer TiO_2 cell proved more effective than the ten layer cell. Two current vs. voltage test curves for this cell are shown in Figure 28. Based on these test runs for the five layer cell and the equations listed in Section 2.2.2, the characteristics of the cell were determined. The cell yielded an average efficiency of 3.86%. It demonstrated an average short circuit current density of 68.9 A/m^2, and an average open circuit voltage of 0.793 V. Its FF averaged 0.71.

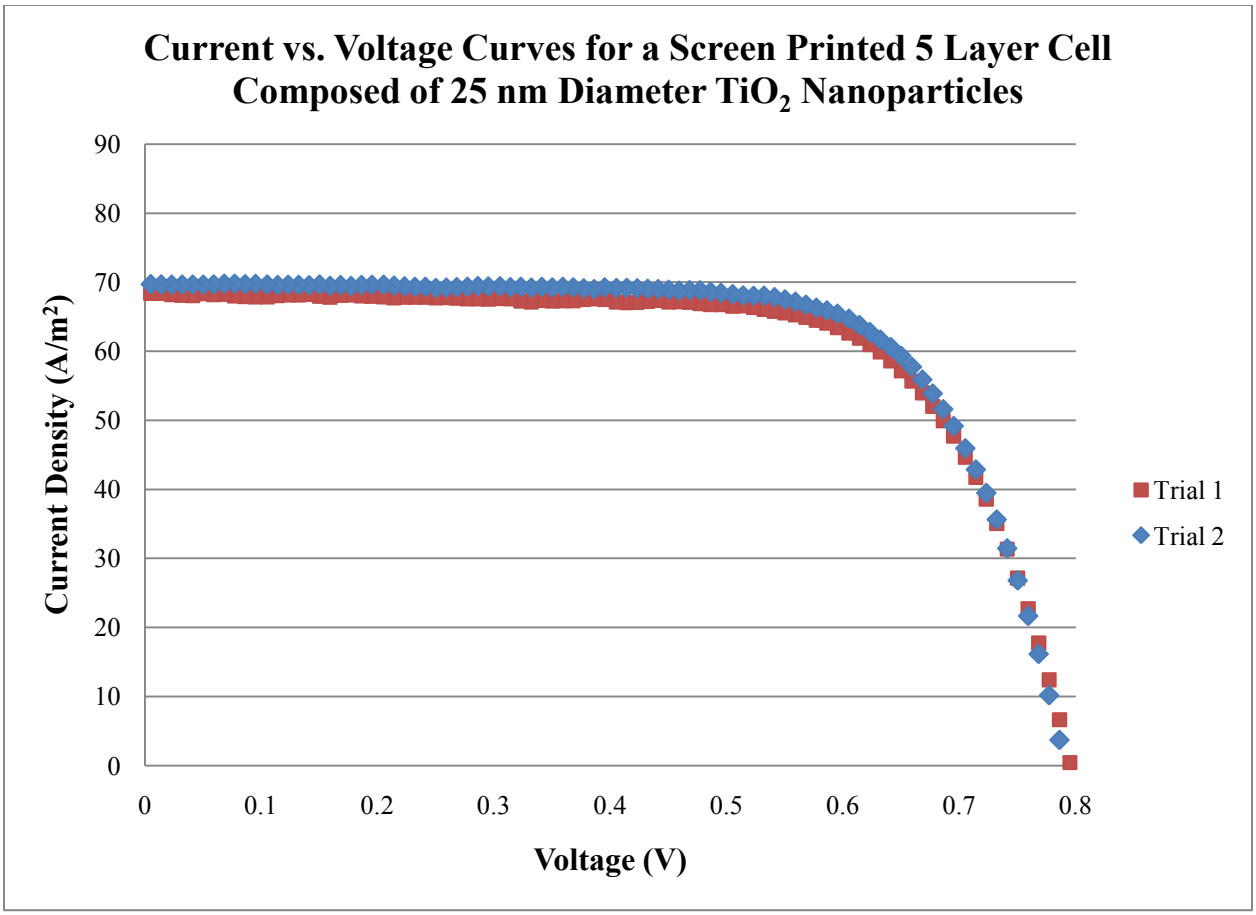

Figure 28: Current vs. voltage curve for screen printed cell.

4.2 Single Layer Doctor Blading

The results of the single layer cell tests using the pastes created in Section 3.2.2 are discussed herein.

4.2.1 Semiconductor Films after Heat Treatment

Both of the titanium dioxide films produced was white, but had different translucencies. The 25 nm diameter nanoparticle film was clearer than the 100 nm diameter nanoparticle film, most likely because of the lower mass of TiO_2 used in the precursor paste. Figure 29 shows the TiO_2 films. Figure 30 shows an AFM image taken of a single layer 25 nm TiO_2 film.

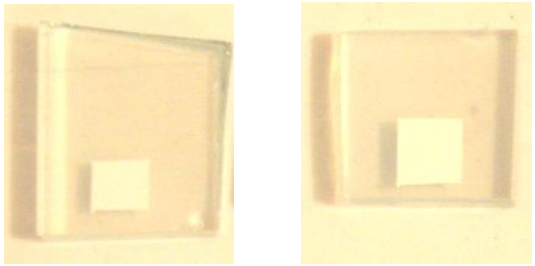

Figure 29: From left to right, films based on 25 nm and 100 nm diameter TiO_2 particles.

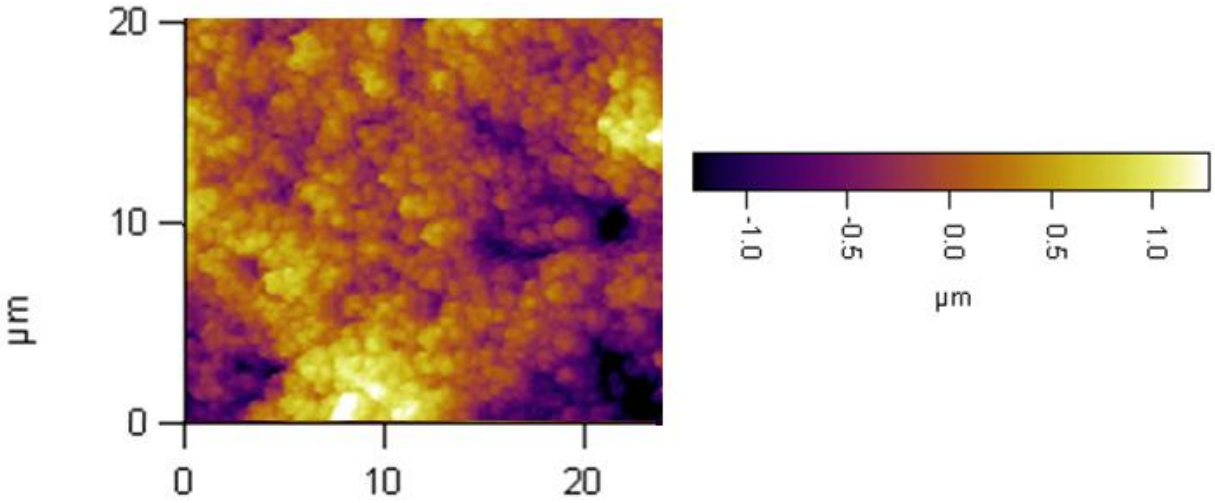

Figure 30: AFM image of the surface of a 25 nm TiO_2 film.

The graphene modified films had a slight gray cast, but the heat treated films were not as darkly tinted as the pastes used to make them. All had a similar degree of transparency. Figure 31 shows the graphene modified films. Figure 32 is an AFM image of a single layer of 25 nm TiO_2 containing 1.0% graphene.

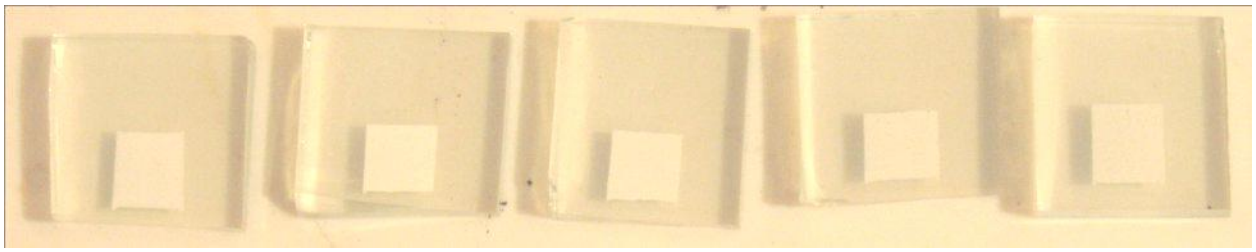

Figure 31: From left to right, films with 0.2, 0.4, 0.6, 0.8, and 1.0 wt% graphene.

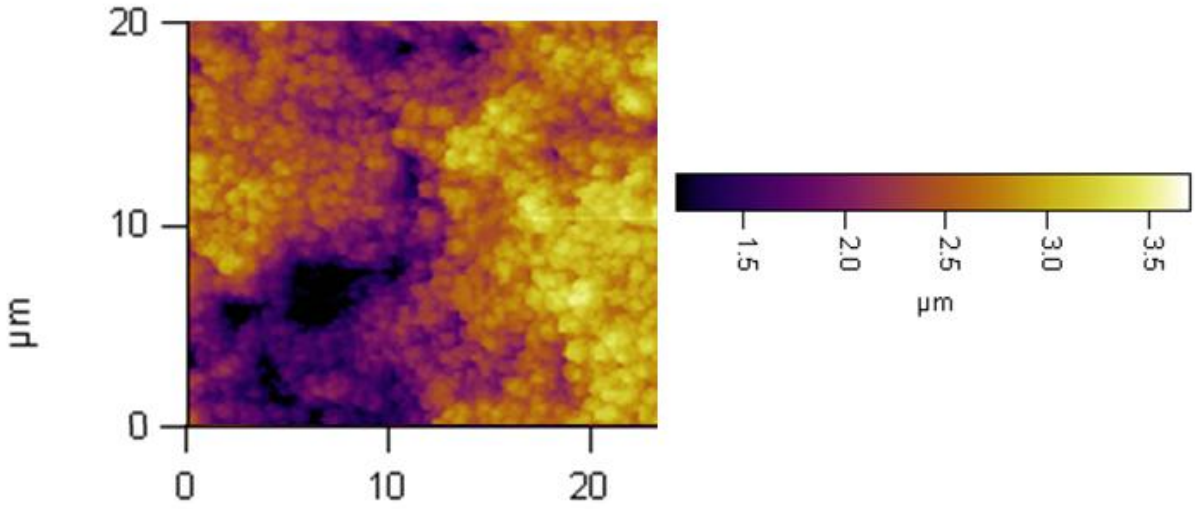

Figure 32: AFM image of the surface of a 25 nm TiO_2 film containing 1.0 wt.% graphene.

Little difference is visible in a comparison of Figure 30 and Figure 32. Both the individual graphene nanoflakes and TiO_2 nanoparticles are too small to be visible at this scale, but it can be observed that the films have a similar porosity on a microscopic scale. The addition of graphene does not appear to have promoted any additional aggregation. If this is the case, then all of the 25 nm TiO_2 pastes should behave in a similar manner when they are applied to a glass surface.

4.2.2 Dye Application

Some of the inherent differences of the films became visible after dyeing. The completed, un-doped TiO_2 films are shown in Figure 33. The dye uptake was clearly lower in the film that consisted of 100 nm diameter nanoparticles. This was predictable, given that larger nanoparticles will tend to have less space between them, and therefore less room for dye to infiltrate.

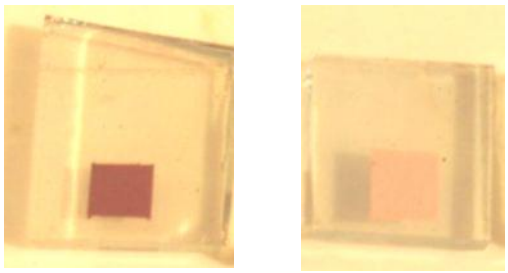

Figure 33: Left to right, dyed films based on 25 nm and 100 nm diameter TiO_2 particles.

Much less variation, if any, can be discerned in the graphene modified films in Figure 34. This is not surprising as all the films were based on 25 nm diameter nanoparticles; the tints of all the graphene films are very similar to the tint of the unaltered 25 nm diameter TiO_2 film. Color comparison is not a definitive indication of dye uptake, but is suggestive.

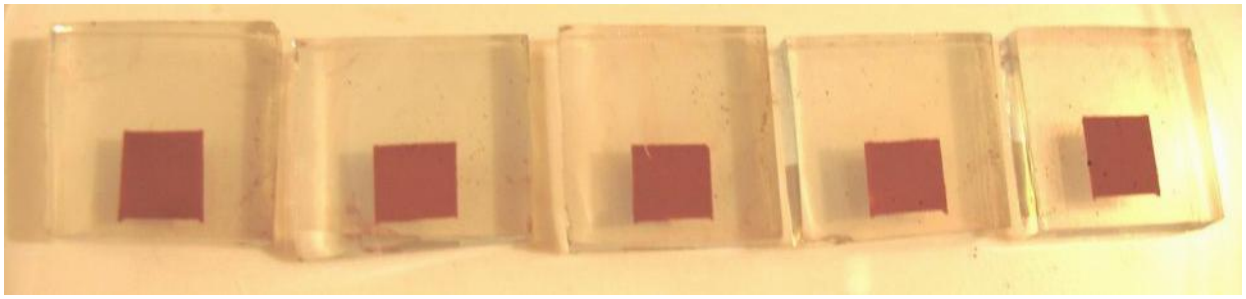

Figure 34: From left to right, dyed films based on with 0.2, 0.4, 0.6, 0.8, and 1.0 wt% graphene.

4.2.3 Testing and Calculated Values

The current density vs. voltage curves for 25 nm and 100 nm based cells appear in Figure 35. The difference is dramatic. The 25 nm TiO_2 cell"s short circuit current density of 46.5 A/m^2 is approximately nine times the 5.3 A/m^2 of the 100 nm TiO_2 cell. The FF and efficiency of the first cell are 0.68 and 2.23% respectively. These values were calculated for the second cell – 0.26 and 0.09% respectively – but may have little meaning because its performance is so unlike the standard curve, which was depicted in Figure 7. However, because the 100 nm TiO_2 paste is intended to act primarily as a light scattering layer, it may still serve its purpose.

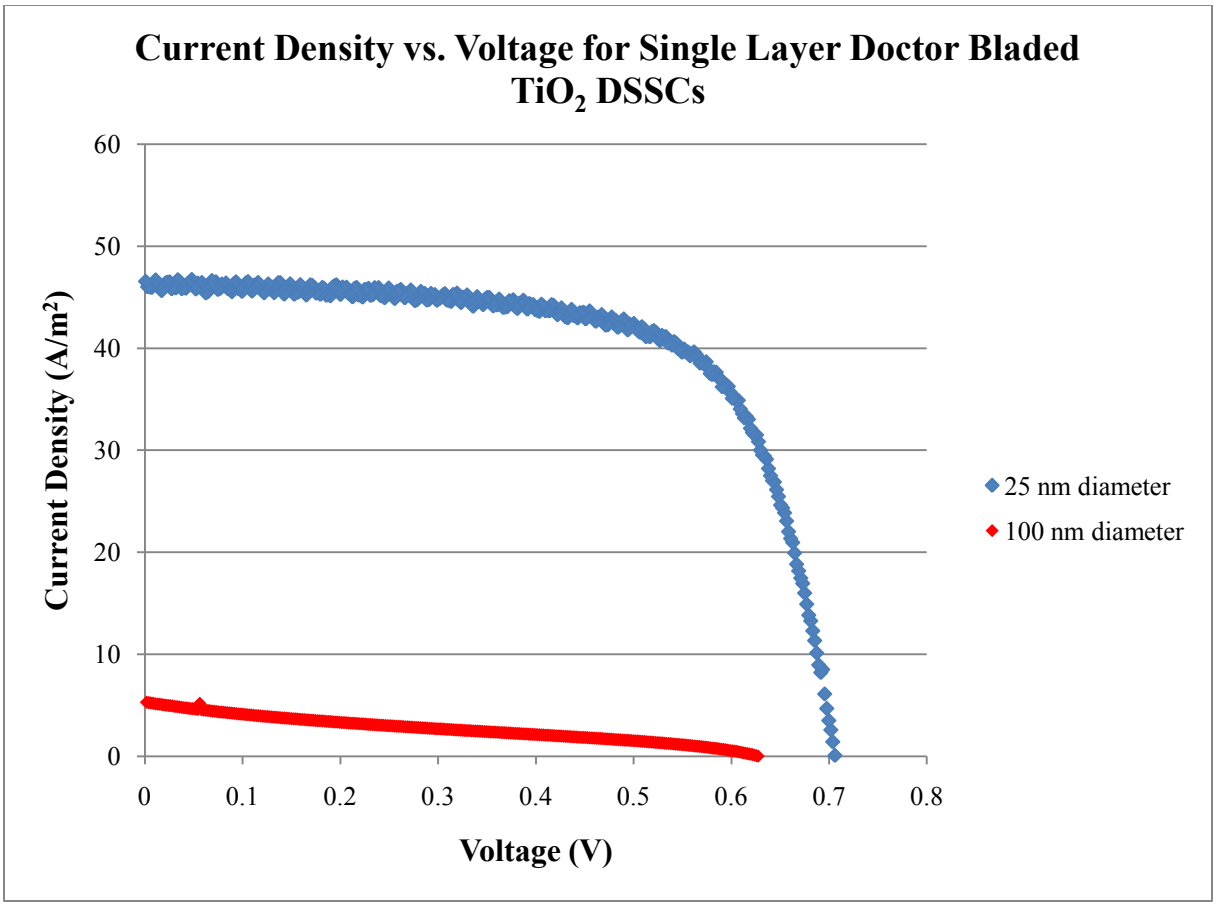

Figure 35: Testing results for single layer doctor bladed TiO_2 cells.

The single layer doctor bladed test results of the graphene containing pastes are depicted in Figure 36. While the calculated characteristics of the single layer graphene containing films will be discussed in conjunction with the multi-layer graphene containing film characteristics in Section 4.6, some striking aspects of the current vs. voltage curves had an impact on the direction of additional research. The shapes of the curves are inconsistent, and the open circuit voltages vary considerably. In particular, the cell containing 0.8% graphene demonstrates a particularly low open circuit voltage. It may have experienced a short circuit during testing if graphene within the film was in contact with both the photo- and counter-electrode glass. A similar phenomenon on a lower scale may also have affected the other cells. For this reason, it

was decided that in the subsequent multi-layer cells, plain TiO_2 layers would be created above and below the graphene layer in each cell to serve as an insulator and prevent short circuits.

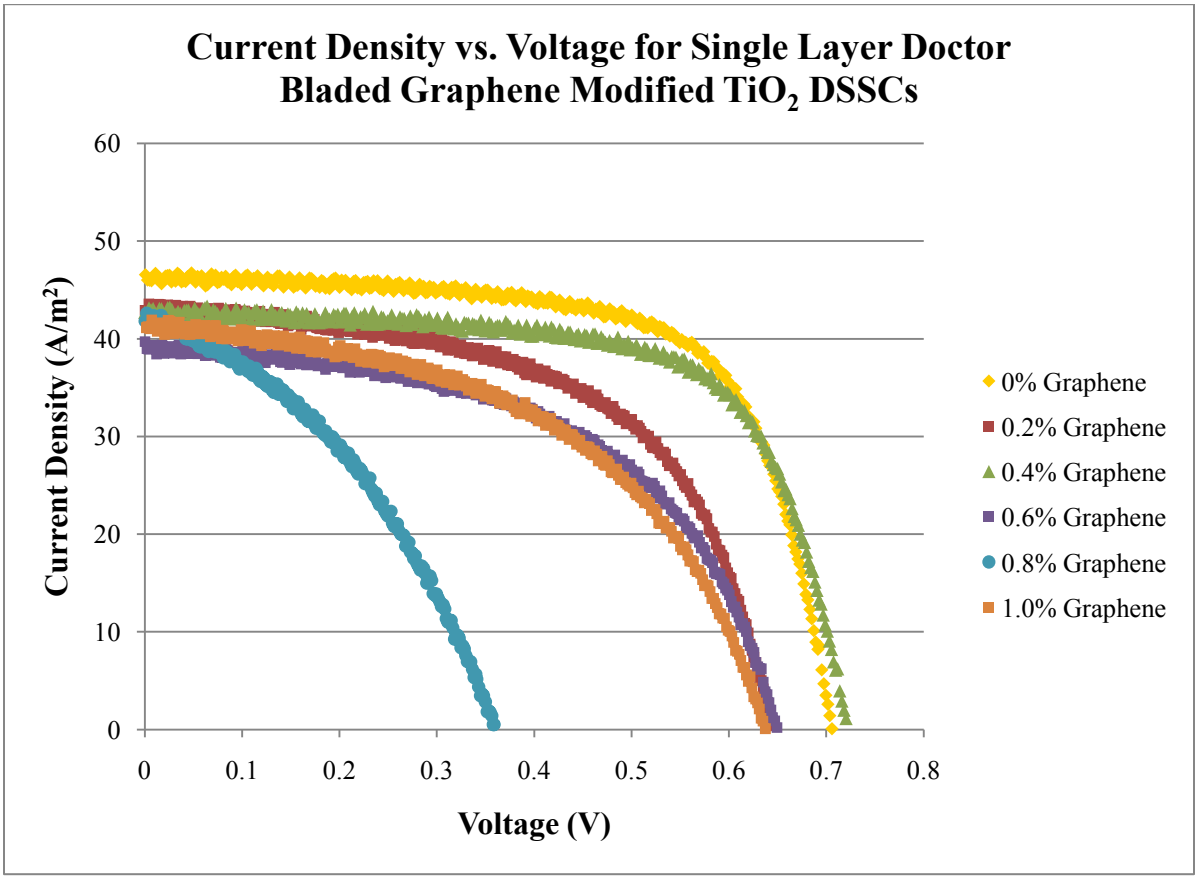

Figure 36: Testing results for single layer doctor bladed graphene containing cells.

4.3 Optimum Thickness Testing

The overall thickness of layered cells can significantly impact their performance as discussed in Section 2.3.5. It was therefore important to determine, where possible, the ideal thickness, in terms of layers, that could be achieved with the multi-layer doctor blading and stamping methods. Based on the results of the single layer doctor blading tests, it was decided that a minimum of three layers would be employed in each subsequent cell.

The multi-layer doctor blading approach produces relatively thick layers, so the intention was to test three, four, five and six layers of thickness. However, all attempts to produce more

than three layers using this method failed due to widespread cracking of the films, as illustrated in Figure 37. This four layer cell had sufficient integrity for testing, but would not be acceptable or consistent for comparisons. Test results for three and four layer cells appear in Figure 38.

Figure 37: Cracked four layer doctor bladed film after dyeing.

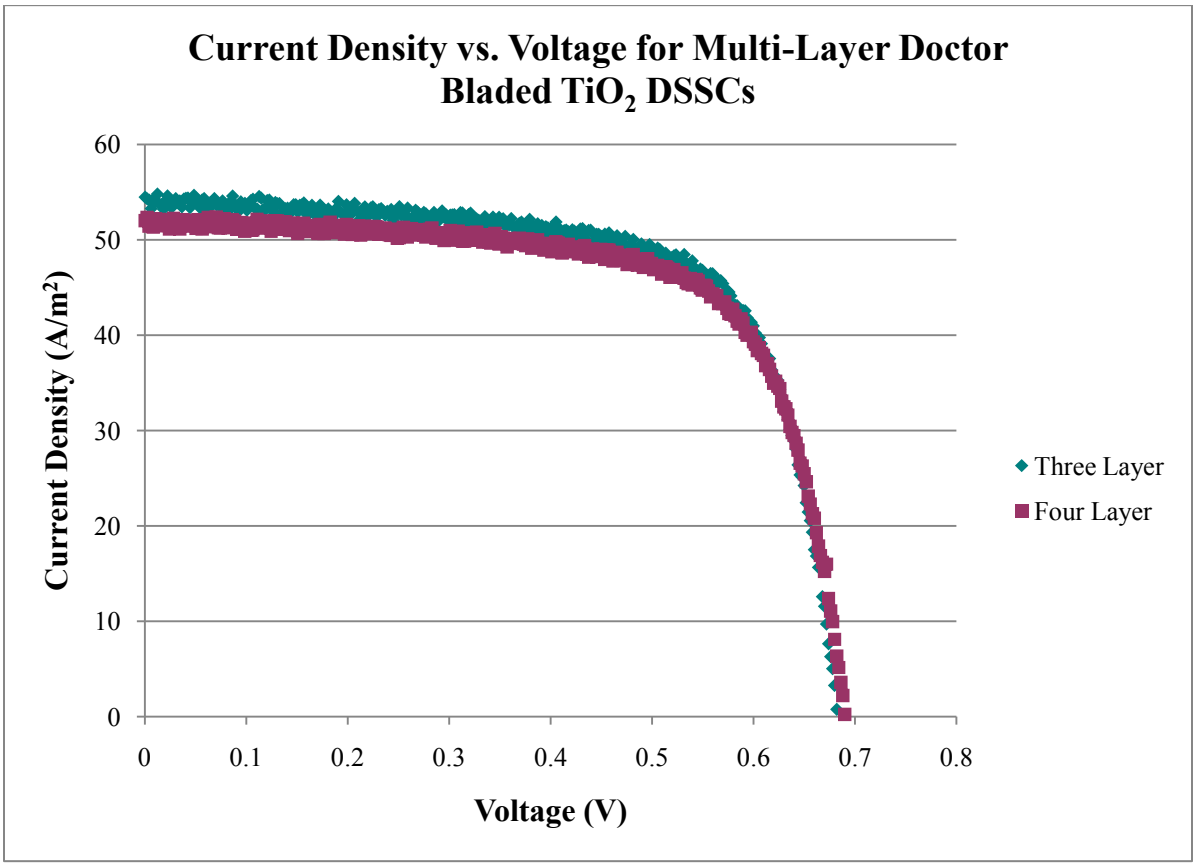

Figure 38: Test results for three and four layer doctor bladed cells.

There is little deviation caused by the addition of the fourth layer. The short circuit current density is reduced from 54.6 to 52.2 A/m^2, the FF from 0.70 to 0.69, and the efficiency from 2.60% to 2.50%. Open circuit voltage increased negligibly from 0.683 to 0.690 V. The three layer cell is superior, so it is the basis of all future multi-layer doctor blading cell comparisons.

The stamping method produced visibly thinner layers, so the decision was made to test four, six, eight, and ten layer 25 nm TiO_2 cells. The results of these tests may be seen in Figure 39. The short circuit current density increases steadily up to eight layers, then falls off at ten layers. Based on this result, all subsequent stamped cells were made eight layers thick. The eight layer reference cell sported an efficiency of 3.92%, a FF of 0.69, and a short circuit current density of 82.7 A/m^2.

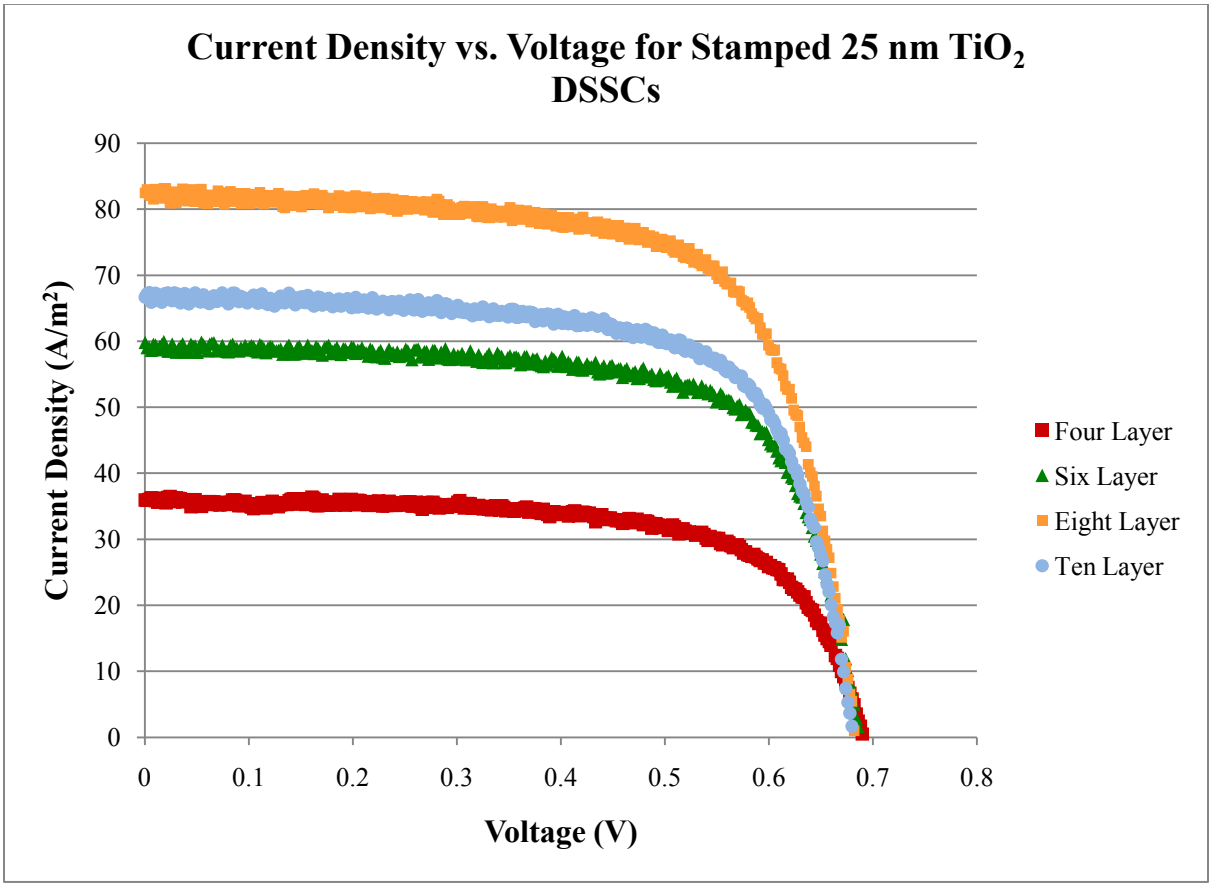

Figure 39: Test results from four, six, eight, and ten layer cells.

4.4 Multi-Layer Doctor Blading

Two sets of multi-layer doctor bladed cells were created using the two formats illustrated in Figure 40. The set on the left is designated 25 nm – X – 25 nm and the set on the right is designated 25 nm – X – 100 nm. The paste represented by the term X varies from 0% to 1.0% graphene.

Figure 40: Arrangement of layers in multi-layer doctor bladed cells.

4.4.1 Semiconductor Films Before and After Dyeing

After heat treatment, the 25 nm – X – 25 nm and 25 nm – X – 100 nm cells were virtually indistinguishable. However, dye application exposed the inherent difference and gave confirmation of the presence of the light scattering layer in the second set of films. As shown in Figure 41, films without a scattering layer had a dark, uniform color. Figure 42 shows the interior side of films with a scattering layer, and Figure 43 shows the exterior layer of the films. The reduced dye absorption in the scattering layer is clearly visible, but the presence of the scattering layer did not inhibit dye absorption in the layers close to the photo-electrode glass.

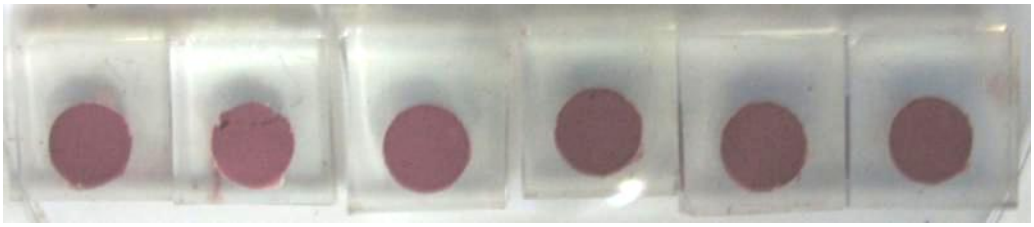

Figure 41: Dyed films without a scattering layer.

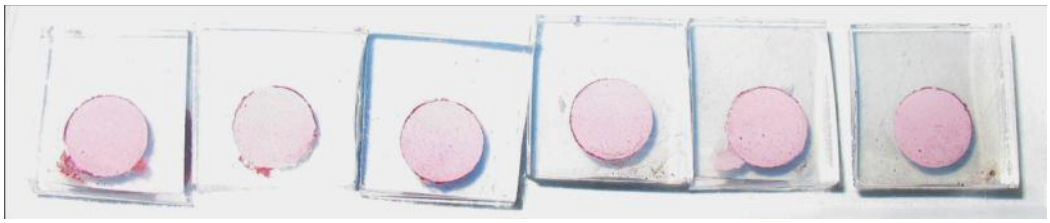

Figure 42: Dyed films with a scattering layer, interior side.

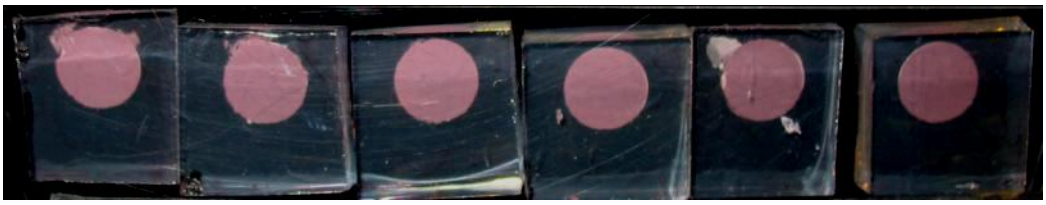

Figure 43: Dyed films with a scattering layer, exterior side.

4.4.2 Testing and Calculated Values

The current density vs. voltage curves for the 25 nm – X – 25 nm cells appear in Figure 55 in the Appendix. The curves for the 25 nm – X – 100 nm cells appear in Figure 56 in the Appendix. The current densities of both sets of cells are compared in Figure 44. The single layer cells exhibited the lowest current densities, and lacked a clear trend. This may be due to short circuits between the graphene and the pieces of glass and, because they are thin, excess light passing through the films unabsorbed. The behavior of the 25 nm – X – 25 nm cells was as anticipated. Current density increased steadily from 0% to 0.8%, then fell off at 1.0%. It is probably around 1.0% content that the graphene begins to block light access to the interior of the cell. Overall, the 25 nm – X – 100 nm cells had lower current densities than the 25 nm – X – 25 nm set, but higher current densities than the single layered cells. The scattering layer is less conductive than the 25 nm layer, so a lower set of current densities is not unreasonable. Within this third set, current densities increased until 0.4%, decreased from 0.4% to 0.8%, then experienced a peak at the final value of 1.0% graphene content. The explanation for this behavior most likely lies in an interaction of the center graphene layer and the scattering layer. It

may be that the decrease in current density from 0.4% to 0.8% graphene occurs because the light is scattered and absorbed in the less conductive layer, and is not returned to the first two layers of the cell. Perhaps the presence of the graphene nanoflakes blocks the return of the light. The sudden spike at 1.0% may mean that at this point the graphene begins to compensate for the lower conductivity of the scattering layer, but the presence of the scattering layer still prevents a short circuit. If this is the case, the presence of a scattering layer between graphene and the counter-electrode might allow the use of higher graphene content than may be employed in cells that lack a scattering layer.

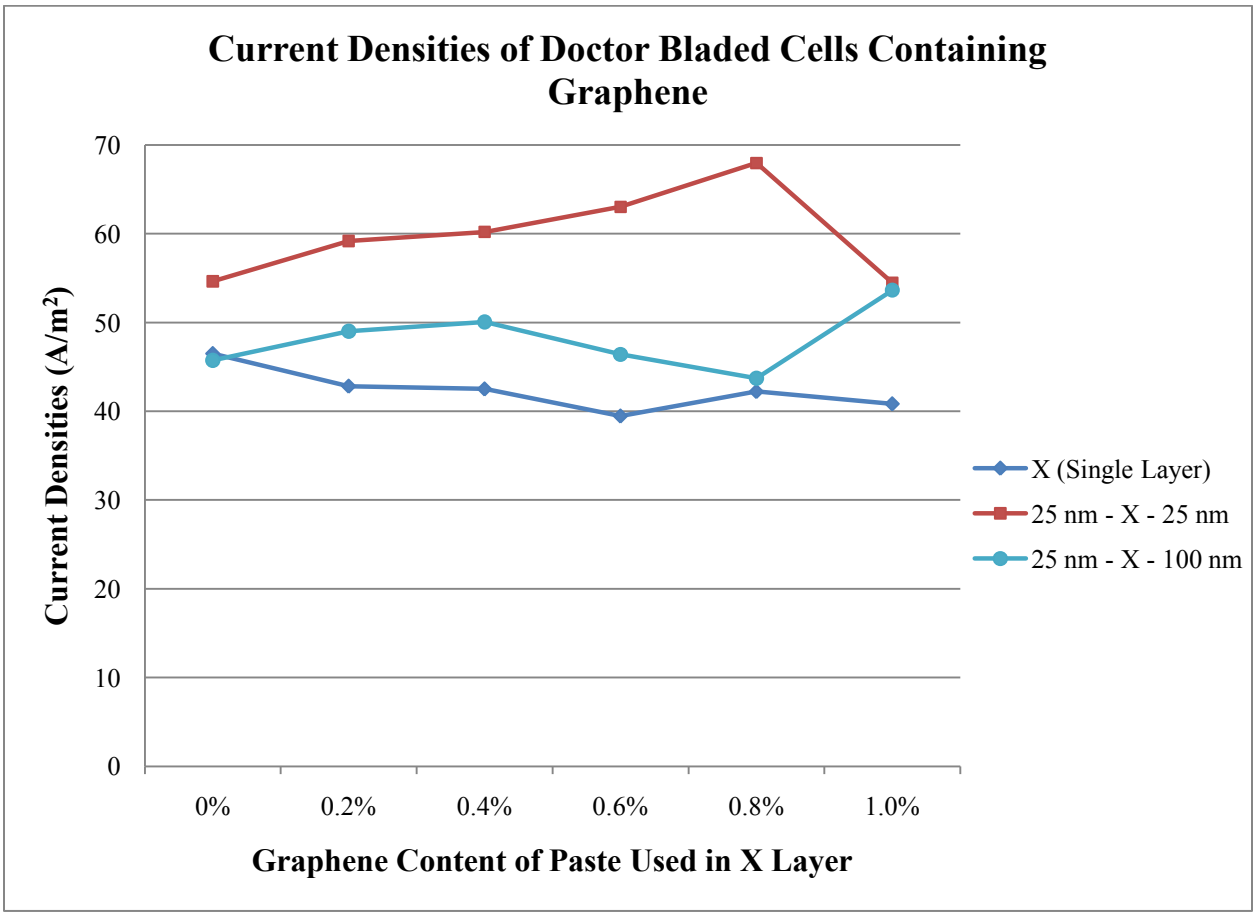

Figure 44: Current densities of single and multi-layer doctor bladed cells containing graphene.

In Figure 45, a comparison between the FF of the single and multi-layer doctor bladed cells is performed. The single layer cells show no clear correlation, but again this is likely due to

short circuiting within them. In general, the 25 nm – X – 25 nm set of cells shows a downward trend from 0% to 1.0% graphene content. The 25 nm – X – 100 nm set of cells also lacks a clear pattern. It may be that the addition of the scattering layer makes the FF less predictable because of variations in the amount of light refracted.

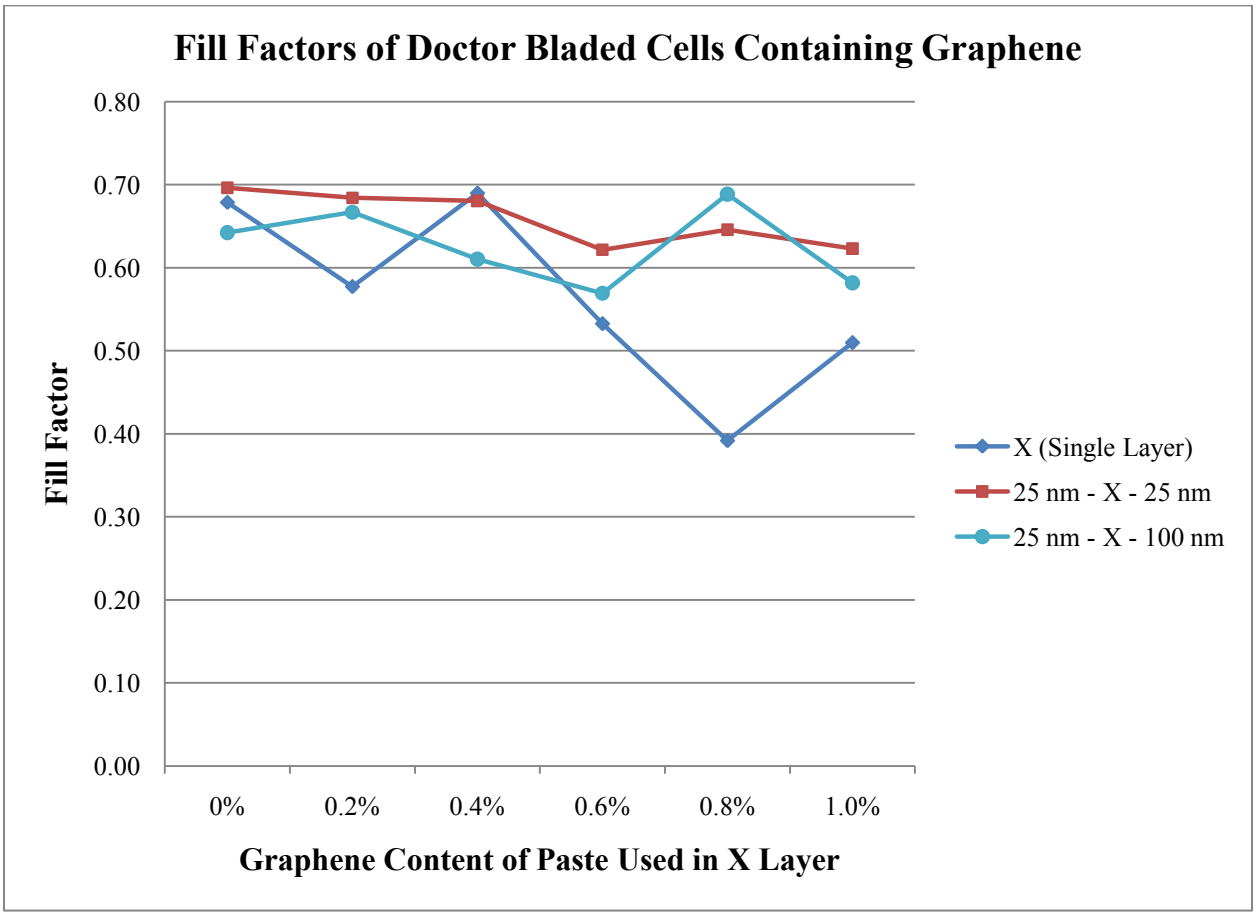

Figure 45: Fill factors of single and multi-layer doctor bladed cells containing graphene.

The efficiencies of the single and multi-layer doctor bladed cells appear in Figure 46. As explained in equation (1.4), efficiency depends on short circuit current, open circuit voltage, and fill factor. As was the case previously, the calculated values for the single layer doctor bladed cells show no pattern. Both the 25 nm – X – 25 nm and 25 nm – X – 100 nm sets show local maxima at 0.2% graphene content and local minima at 0.6% graphene content. The variation in the pattern of efficiencies of the first set compared to the trend visible in the current densities is

primarily due to inconsistencies in open circuit voltage between cells. As Figure 55 in the Appendix shows, there is a spread between the x-intercepts of the 25 nm – X – 25 nm format cells; it ranges from 0.643 to 0.703 V. In Figure 56 in the Appendix, which shows the performance of the 25 nm – X – 100 nm cells, there is much less V_{OC} change, 0.660 to 0.685 V, which may be a result of the scattering layer. For this reason, the efficiencies of this set of DSSCs follow a pattern much closer to that of their current densities.

As a whole, the efficiencies of the 25 nm – X – 25 nm cells are greater than those of the 25 nm – X – 100 nm cells. The maximum efficiency of any of the cells was 2.88%, for the 0.8% cell that lacked a scattering layer. A comparison of calculated values from the multi-layer doctor blading approach to those from the stamping method will be performed in Section 4.6.

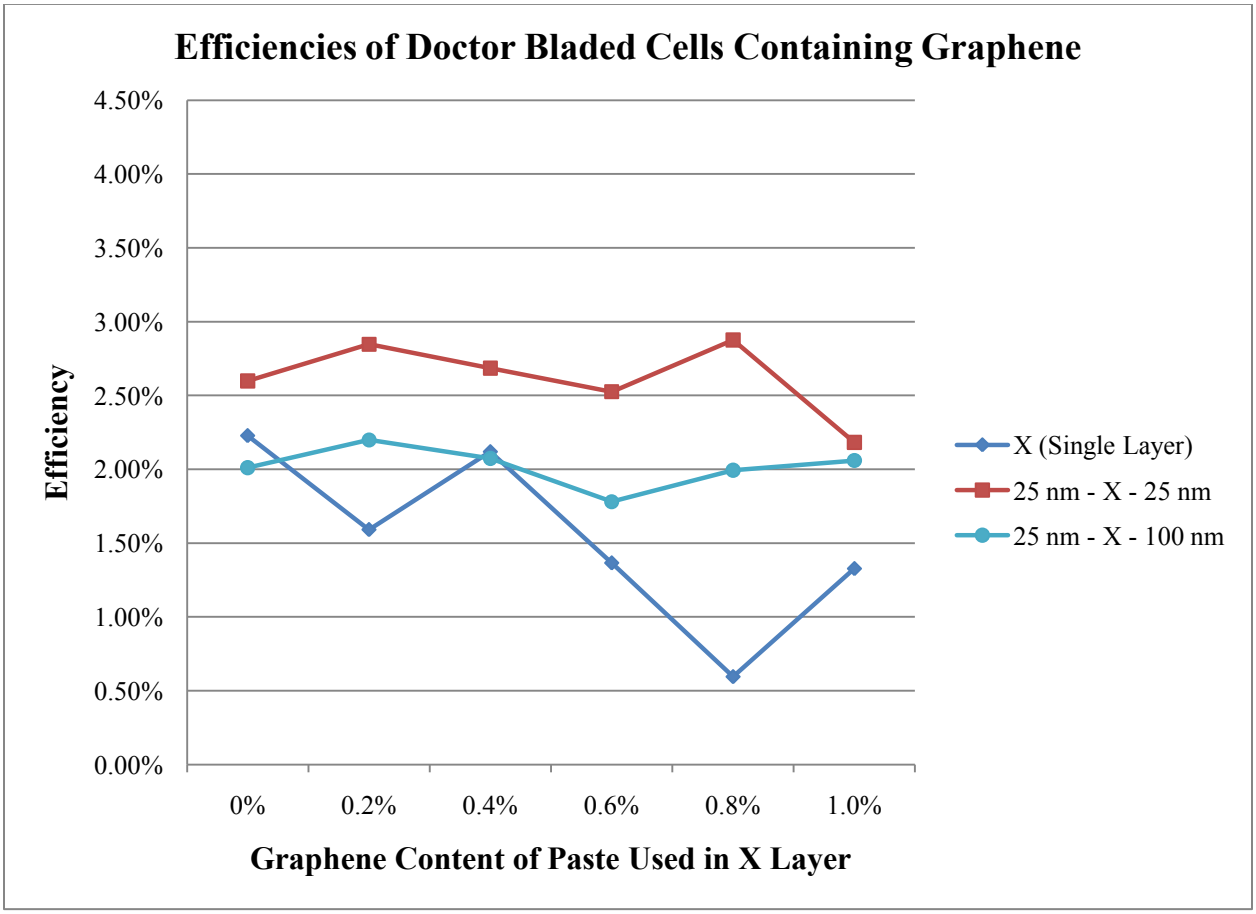

Figure 46: Efficiencies of single and multi-layer doctor bladed cells containing graphene.

4.5 DSSC Performance – Stamping Method

Two sets of stamped cells were created using the two formats illustrated in Figure 47.

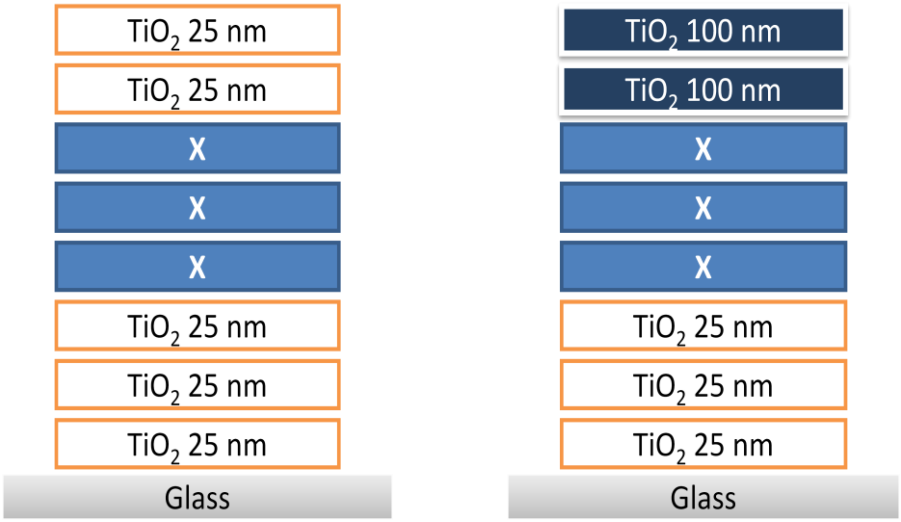

Figure 47: Arrangement of layers in stamped cells.

The set on the left is designated 25 nm (3L) – X (3L) – 25 nm (2L) and the set on the right is designated 25 nm (3L) – X (3L) – 100 nm (2L). The term in parentheses refers to the number of layers of each paste. The paste represented by the term X varies from 0% to 1.0% graphene.

4.5.1 Semiconductor Films Before and After Dyeing

Like the multi-layer doctor bladed films, the absence or presence of a scattering layer was not detectable after heat treatment, but became clear after dyeing. Figure 48 shows semiconductor films in the 25 nm (3L) – X (3L) – 25 nm (2L) arrangement. Figure 49 shows films in the 25 nm (3L) – X (3L) – 100 nm (2L) arrangement.

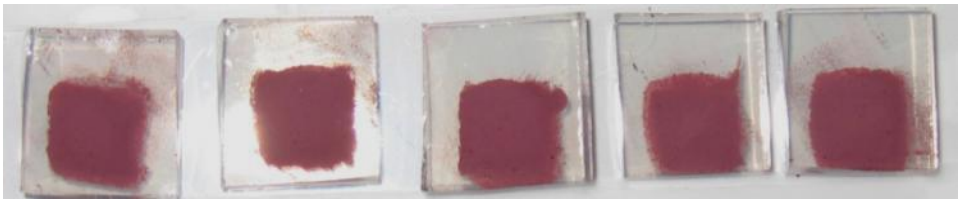

Figure 48: Dyed, stamped cells without a scattering layer.

Figure 49: Dyed, stamped cells with a scattering layer.

One aspect of the stamping method that becomes clear in these images is the tendency of stamped layers to spread out, creating a feathering pattern, so that the edges of layers are not necessarily lined up. Because the lower, graphene containing layers are not fully insulated, there is a potential for them to carry current to the edges and to create a short circuit with the counter-electrode. For this reason, two additional stamped sets of films were created. These had the same layer arrangements as the first two sets, 25 nm (3L) – X (3L) – 25 nm (2L) and 25 nm (3L) – X (3L) – 100 nm (2L). However, before stamping commenced, a piece of tape with a 0.4763 cm diameter hole in the center, identical to the type used for multi-layer doctor blading, was placed on the surface of the glass. Stamping proceeded, and the tape was left in place for all eight layers and each of the 125 °C heat treatments. These two additional sets of stamped cells will be referred to as „masked" to differentiate them from the previous sets.

After the eighth layer and heat treatment, the tape was removed. No visible damage to the edges of the film could be seen, but the tape left an adhesive residue on the surface of the glass, most likely because of the exposure to heat. During the stepped heat treatment used to sinter the films, the residue turned brown and began to decompose, as shown in Figure 50. By the end of the 450 °C stage of the heat treatment, the residue had all but disappeared, as shown in Figure 51. The completed, dyed masked cells appear in Figure 52 and Figure 53. It is worth noting that, masked or unmasked, the surface of the stamped cells was very rough, so much so

that air bubbles became trapped on it during the placement of the counter-electrode. They could not be removed when the electrolyte solution was added.

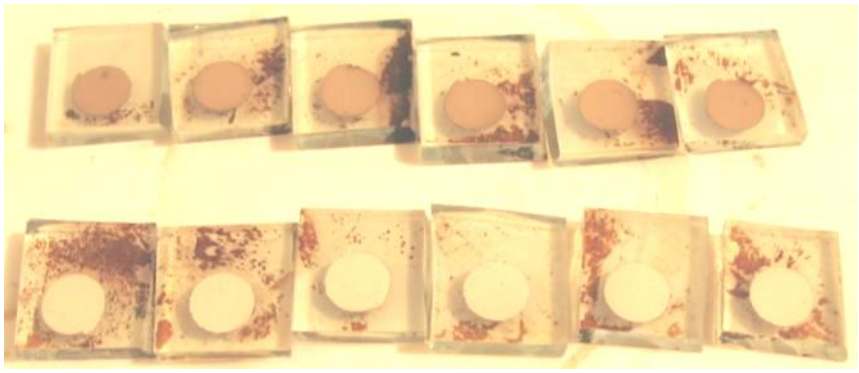

Figure 50: Adhesive residue on the glass decomposing.

Figure 51: Glass slides after the adhesive residue has burned away.

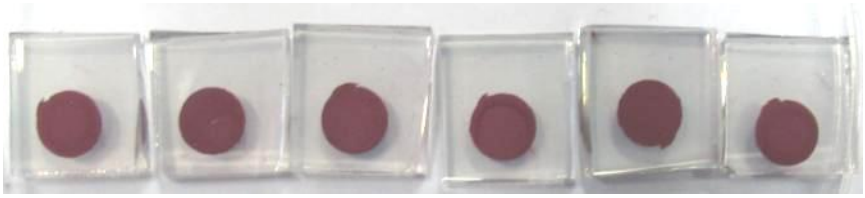

Figure 52: Stamped, masked cells of the format 25 nm (3L) – X (3L) – 25 nm (2L).

Figure 53: Stamped, masked cells of the format 25 nm (3L) – X (3L) – 100 nm (2L).

4.5.2 Testing and Calculated Values

The current density vs. voltage curves for the 25 nm (3L) – X (3L) – 25 nm (2L) cells appear in Figure 57 in the Appendix. The curves for the 25 nm (3L) – X (3L) – 100 nm (2L) cells appear in Figure 58 in the Appendix. The curves for the 25 nm (3L) – X (3L) – 25 nm (2L) masked cells appear in Figure 59 in the Appendix. The curves for the 25 nm (3L) – X (3L) – 100 nm (2L) masked cells appear in Figure 60 in the Appendix. The current densities of all four sets of cells appear in Figure 54. The FF of the cells appear in Figure 61 in the Appendix. The efficiencies of the cells appear in Figure 62 in the Appendix.

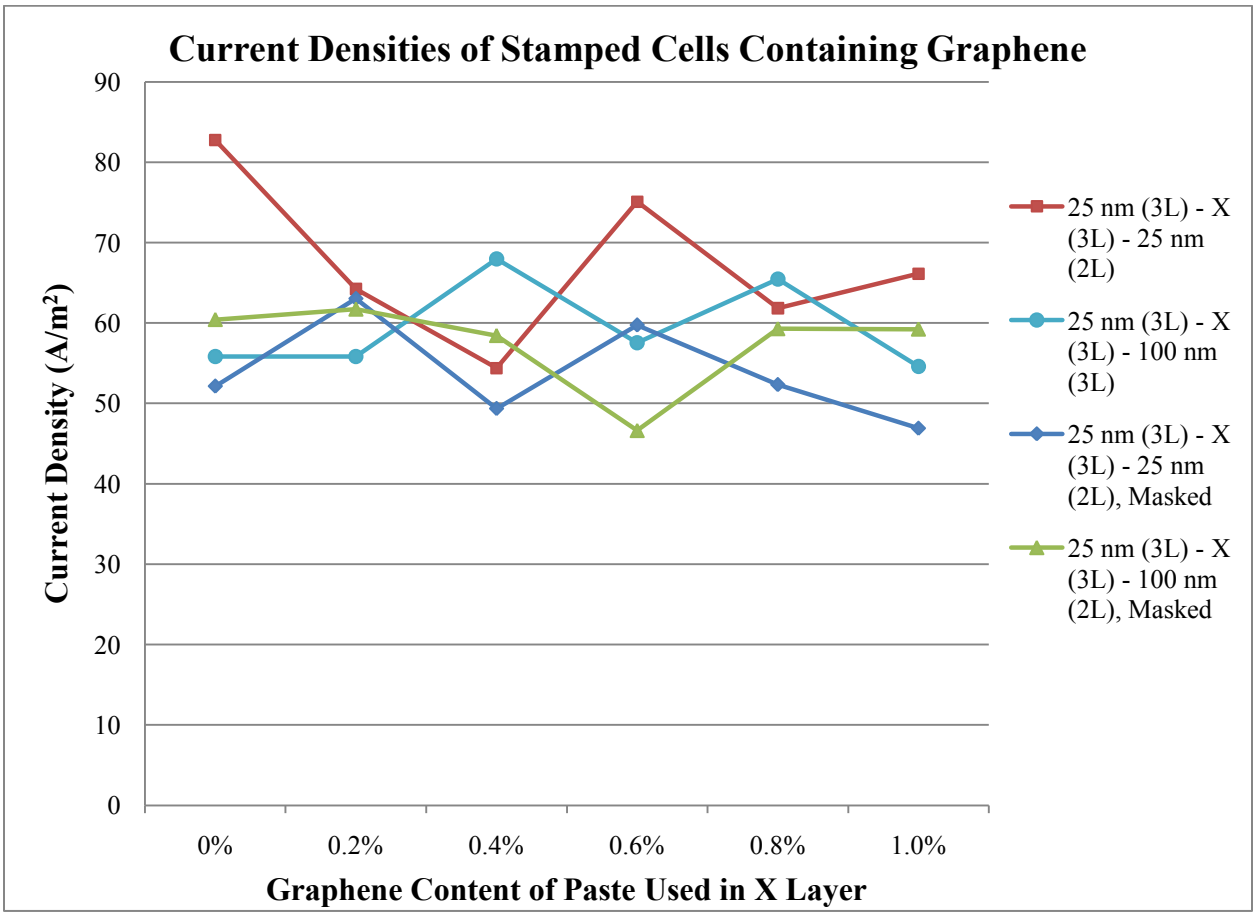

Figure 54: Current densities of stamped cells containing graphene.

In examining the data derived from the stamped cells, no trends emerge in any of the calculated values. The data calculated for current density in Figure 54 are indicative of the

results for all of the cell characteristics. Even for TiO_2 cells containing no graphene, the current densities vary from 52.1 to 82.7 A/m^2 and the efficiencies vary from 1.98% to 3.92%. Even cells with identical layer structures show no consistency. Masking the cells with tape also had no discernible impact on standardization. The same graphene and TiO_2 pastes were used for the stamped cells as were used in the doctor blading cells, which did not show anything approaching this level of variation. It seems that there is some inherent variable in the stamping method that is not being controlled. It may be the porous structure of the sponges used for stamps, a magnified view of which was shown in Figure 23, is the issue. The pores are microscopic and of variable size. They could be creating unusual structural formations or groupings that are not repeated between different cells. It may be that internal cell porosity varies greatly in stamped cells. A comparison of results from all three methods will be performed in Section 4.6.

4.6 Comparison of Multi-layer Film Characteristics

As stated previously, the screen printed TiO_2 reference film yielded an average efficiency of 3.86%, an average short circuit current density of 68.9 A/m^2, an average open circuit voltage of 0.793 V, and a FF that averaged 0.71. It was tested using N-719, and the multi-layer doctor bladed and stamped cells were tested using N-3. N-719 has been shown to yield 0.9% higher efficiencies and 0.9% higher open circuit voltages that N-3 dye when used on similar cells. N-3 dye by comparison has led to 1% higher current densities than N-719 [60].

Multi-layer doctor bladed cells do not perform as well as the screen printed sample. The TiO_2 cell without graphene or a scattering layer had a short circuit current density of 54.6 A/m^2, and the highest short circuit current density, achieved by a cell with 0.8% graphene and no scattering layer, was 68.0 A/m^2. The open circuit voltages did not climb above 0.703 V, which is at the edge of the difference that can be accounted for by the 1% margin. The lower open circuit

voltages are not accounted for by the margin. Efficiencies are also lower, with the maximum of 2.88% also achieved by the 0.8% graphene cell without a scattering layer.

Stamped cells have highly variable performance. The best cell, involving an unmasked TiO_2 film without a scattering layer, exhibited a 3.92% efficiency. This is superior to that achieved by the screen printed cell. This stamped cell also boasted the highest short circuit current, 82.7 A/m^2, which was significantly higher than that of either the screen printed or doctor bladed cells, and is not accounted for by the difference in dyes. Its open circuit voltage was lower, 0.683 V, but this did not prevent it from being more efficient. However, the pattern of increasing current density and efficiency anticipated based on this result did not manifest. The next highest stamped efficiency was 3.13%, reached by an unmasked 0.4% graphene content cell with a scattering layer.

4.7 Cost Analysis

To assess the competitiveness of a DSSC produced by the methods discussed in Section 3.2.2, an analysis was performed to estimate cost per experimental sized cell. The results of material cost analysis are shown in Table 4. One complete cell costs approximately $0.85. Because each of the methods produced cells from the same precursor chemicals, material cost does not vary between cells. Graphene addition adds a negligible cost at the quantities used. Any variation is caused by the need for specialized equipment. Multi-layer doctor blading requires Scotch tape and glass stirring rods. Glass stirring rods are a standard item of lab equipment, and it is presumed that any lab endeavoring to make DSSCs will have them on hand. A bulk order of Scotch tape (ten rolls, each 27.7 yds long) costs $22.99 [61]. Assuming an average of 3.0 in. of tape per cell, the added expense is less than $0.01, for a total cost of at most $0.86.

TABLE 4

COST ANALYSIS OF EXPERIMENTAL SIZED TITANIUM DIOXIDE BASED DSSC.

	Material	Bulk Qty.	Bulk Price	Batch Quantity	Price per Batch	Total Batch Cost	Per Cell Qty.	Per Cell Price
TiO_2 Paste	TiO2 (< 25 nm diameter)	50 g	$93.90	0.423 g	$0.79	$1.95	0.010 g	$0.01
	Terpineol	100 mL	$53.10	1.2 mL	$0.64			
	E. Cellulose (5-15 mPas)	250 g	$117.50	0.113 g	$0.05			
	E. Cellulose (30-50 mPas)	250 g	$73.10	0.088 g	$0.03			
	Ethanol	500 mL	$52.00	4.281 mL	$0.45			
Chloroplatinic Acid Solution	H_2PtCl_6	0.25 g	$52.40	0.002 g	$0.42	$0.52	0.083 mL	$0.04
	Ethanol	500 mL	$52.00	1 mL	$0.10			
Dye Solution	N-3 Dye	0.25 g	$295.00	0.021 g	$24.78	$26.34	0.167 mL	$0.29
	Ethanol	500 mL	$52.00	15 mL	$1.56			
Electrolyte Solution	Acetonitrile	2 L	$127.50	8.5 mL	$0.54	$21.67	0.083 mL	$0.18
	Valeronitrile	100 g	$56.30	1.5 mL	$1.06			
	BMII	5 g	$54.20	1.597 g	$17.31			
	Iodine	25 g	$56.80	0.076 g	$0.17			
	Guanidine thiocyanate	25 g	$22.90	0.118 g	$0.11			
	4-tert-butylpyridine	25 g	$91.50	0.676 g	$2.47			
Substrate	ITO Glass	100 pcs	$65.00	0.25 pcs	$0.16	$0.16	0.5 pcs	$0.33
					Total Cost Per Cell			$0.85

The sponges needed for stamping cost $1.72 for every 32 sponges. Each sponge can be cut into at minimum four stamps. Up to three stamps could be used per cell. The price per cell for sponges is therefore $0.04, which raises the total to $0.89 per cell. Screen printing has the most significant start-up price for equipment. A small table-top screen printer like the one employed in these experiments costs around $15, with another $10 needed for a squeegee. The added price per cell depends on the number of cells made. If it is 100, then the added cost is $0.25 per cell, for a total cost of $1.10 per cell. A professional, customizable screen printer can cost much more.

CHAPTER 5

CONCLUSIONS & FUTURE WORK

5.1 Conclusions

In this thesis, two methods of creating multi-layer porous films for DSSCs were examined. They were designed as possible alternatives for screen printing in laboratory settings. The same precursor chemicals used for screen printing were employed in both the alternative methods, which were designated multi-layer doctor-blading and stamping. Both alternatives are simple and inexpensive. The cells produced by these two methods were compared to a sample screen printed cell, with mixed results. The multi-layer doctor bladed method is less flexible than the screen printing method in terms of the number of layers that can be used with standard Scotch tape. Unless thinner tape can be found that allows more structural variation, it does not appear that the multi-layer doctor blading approach is suitable for further experimentation. Its relatively low performance is also an indicator that it is not the best means by which to study DSSCs. The stamping method yielded the highest efficiency cell created during the course of these experiments. It also has potential because it allows the creation of a variety of layers within the same cell. However, some variety of inherent variation in the stamping method prevented repetition of this success. In order for it to truly become an effective method for creating DSSCs in laboratory settings, the source of this variation must be found and standardized.

5.2 Future Work

The stamping method appears the most viable as a screen printing alternative, but before it can be employed, a means of standardization must be identified. This would involve detailed structural analysis of the films produced with this method to determine the extent of the

variations and to confirm or disprove the theory that structural inconsistencies are responsible for the lack of repeatability in the results. If this is found to be the case, then a means of creating a repeatable structure by stamping must be found. This may require the discovery or development of a foam sponge material that is nanoporous rather than microporous. A nanoporous sponge may allow for a more controlled paste application. It would also be worthwhile to see what effect a titanium tetrachloride treatment would have on film structure and performance if this could be arranged.

REFERENCES

REFERENCES

[1] A. Luque and S. Hegedus, "Status, Trends, Challenges and the Bright Future of Solar Electricity from Photovoltaics," in *Handbook of Photovoltaic Science and Engineering*, A. Luque and S. Hegedus, Eds., ed Chicester: John Wiley & Sons, 2003, pp. 1-43.

[2] German Foundation for Solar Energy. (2010, 5-30-2010). "Photovoltaics: Solar Electricity and Solar Cells in Theory and Practice." *2010(5-30-2010)*. Available: http://www.solarserver.de/wissen/photovoltaik-e.html

[3] B. O'Regan and M. Gratzel, "A low-cost, high-efficiency solar cell based on dye-sensitized colloidal TiO_2 films," *Nature,* vol. 353, pp. 737-740, 1991.

[4] M. Grätzel, "Molecular photovoltaics that mimic photosynthesis," *Pure Applied Chemistry,* vol. 73, pp. 459-467, 2001.

[5] A. R. Jha, *Solar Cell Technology and Applications*. Boca Raton: CRC Press, 2010.

[6] G. M. Hopkins, "Reminiscences of Daguerreotypy," *Scientific American* vol. 56, pp. 47, 52, 1887.

[7] M. Matsumura*, et al.*, "Dye-sensitization on the Photocurrent at Zinc Oxide Electrode in Aqueous Solution," *Bulletin of the Chemical Society of Japan,* vol. 50, pp. 2533-2537, 1977.

[8] J. L. Gray, "The Physics of the Solar Cell," in *Handbook of Photovoltaic Science and Engineering*, A. Luque and S. Hegedus, Eds., ed Chicester: John Wiley & Sons, 2003, pp. 61-112.

[9] G. Ghione, *Semicondutor Devices for High-Speed Optoelectronics*. Cambridge: Cambride University Press, 2009.

[10] K. Hara and H. Akarakawa, "Dye-sensitized Solar Cell," in *Handbook of Photovoltaic Science and Engineering*, A. Luque and S. Hegedus, Eds., ed Chicester: John Wiley & Sons, 2003, pp. 663-700.

[11] R. Corkish, "Solar Cells," in *Encyclopedia of Energy*. vol. 5, C. J. Cleveland, Ed., ed: Elsevier, 2004, pp. 545-557.

[12] G. Wang and Y. Lin, "Novel counter electrodes based on NiP-plated glass and Ti plate substrate for dye-sensitized solar cells," *Journal of Material Science* vol. 42, pp. 5281-5285, 2007.

[13] R. Chang, *General Chemistry: The Essential Concepts*, 3 ed. Boston: McGraw Hill, 2003.

[14] (2008, 5-30-2010). DGAP-News: Dyesol Limited:Record Efficiency for Cells Using Dyesol Paste. Available: http://www.ad-hoc-news.de/drucken--/de/Wirtschaft-Boerse/Marktberichte/19367079

[15] W. Gruener. (2009, 5-30-2010). Fraunhofer claims world record in solar cell efficiency - 41.1%. Available: http://www.tgdaily.com/trendwatch-features/41224-fraunhofer-claims-world-record-in-solar-cell-efficiency-411

[16] H. Han, "A novel hybrid nanocrystalline TiO2 electrode for the dye-sensitized nanocrystalline solar cells," *Journal of Materials Science,* vol. 40, pp. 4921-4923, 2005
.

[17] P. V. V. Jayaweera*, et al.*, "Why Grätzel‟s Cell Works so Well," *Inorganica Chemica Acta,* vol. 368, pp. 707-711, 2008.

[18] M. Quintana*, et al.*, "Comparison of Dye-Sensitized ZnO and TiO2 Solar Cells: Studies of Charge Transport and Carrier Lifetime," *Journal of Physical Chemistry C,* vol. 111, pp. 1035-1041, 2007.

[19] S. Banerjee*, et al.*, "Physics and chemistry of photocatalytic titanium dioxide: Visualization of bactericidal activity using atomic force microscopy," *Current Science,* vol. 90, pp. 1378-1383, 2006.

[20] B. Mills, "Rutile-unit-cell-3D-balls," Wikipedia, 2007, Ball-and-stick model of part of the crystal structure of rutile, one of the mineral forms of titanium dioxide, TiO2.

[21] B. Mills, "Anatase-unit-cell-3D-balls," Wikipedia, 2007, Unit cell of anatase.

[22] T. Lindgren*, et al.*, "Photoelectrochemical and Optical Properties of Nitrogen Doped Titanium Dioxide Films Prepared by Reactive DC Magnetron Sputtering," *J. Phys. Chem. B,* vol. 107, pp. 5709-5716, 2003.

[23] Q. Yao*, et al.*, "Nd-Doped TiO2 Nanorods: Preparation and Application in Dye-Sensitized Solar Cells," *Chem. Asian J.,* vol. 1, pp. 737 – 741, 2006.

[24] M. Grätzel, "Light and Energy, Electric Power Generation by Dye Sensitized Solar Cells," presented at the International Conference on the Industrialization of DSC, Canberra, 2006.

[25] B. Mills, "Carboxylate-resonance-2D," Wikipedia, 2009, Modified version of structural description of the delocalisation of electrons in the pi system of a carboxylate anion.

[26] "Phosphonate," Wikipedia, 2006, Phosphonate.

[27] "Brenzcatechin," Wikipedia, 2008, Structure of Pyrocatechol.

[28] S. Prahl. Rose Bengal. Available: http://omlc.ogi.edu/spectra/PhotochemCAD/html/rosebengal.html

[29] A. L. Davies. (2005). *Energy Harvesting Materials*. Available: http://www.knovel.com.proxy.wichita.edu/web/portal/basic_search/display?_EXT_KNOVEL_DISPLAY_bookid=1784&_EXT_KNOVEL_DISPLAY_fromSearch=true&_EXT_KNOVEL_DISPLAY_searchType=basic

[30] A. D. McNaught and A. Wilkinson. Compendium of Chemical Terminology [Online]. Available: http://old.iupac.org/publications/books/author/mcnaught.html

[31] SolaronixSA. (2009, July 20th, 2009). *Solaronix.com*. Available: http://www.solaronix.com/

[32] Dyesol. (2005-2008, July 20th, 2009). *Dyesol.com*. Available: http://www.dyesol.com

[33] N. J. Cherepy, *et al.*, "Ultrafast Electron Injection: Implications for a Photoelectrochemical Cell Utilizing an Anthocyanin Dye-Sensitized TiO2 Nanocrystalline Electrode," *Journal of Physical Chemistry B,* vol. 101, pp. 9342-9351, 1997.

[34] H. J. Lee, *et al.*, "CdSe Quantum Dot-Sensitized Solar Cells Exceeding Efficiency 1% at Full-Sun Intensity," *Journal of Physical Chemistry C,* vol. 112, pp. 11600 –11608, 2008.

[35] U. S. Department of Energy. (2006, July 17th, 2009) "Electrical Contacts." Available: http://www1.eere.energy.gov/solar/electrical_contacts.html

[36] T. Yuji and Y.-M. Song, "Surface Treatment of TiO2 Films by Pulse Plasma for Dye-Sensitized Solar Cells Application," *IEEE Transactions on Plasma Science* vol. 35, pp. 1010-1013, 2007.

[37] J. Jiu, *et al.*, "Dye-sensitized solar cell based on nanocrystalline TiO2 with 3–10 nm in diameter," *Journal of Materials Science: Materials in Electronics* vol. 18, pp. 41-45, 2007.

[38] S. Ito, *et al.*, "Fabrication of thin film dye sensitized solar cells with solar to electric power conversion efficiency over 10%," *Thin Solid Films,* vol. 516, pp. 4613–4619, 2008.

[39] T. Tesfamichael, "Investigations of dye-sensitised titania solar cell electrode using confocal laser scanning microscopy," *Journal of Materials Science,* vol. 38, pp. 1721-1726, 2003.

[40] K. Tennakone*, et al.*, "An efficient dye-sensitized photoelectrochemical solar cell made from oxides of tin and zinc," *Chem. Commun.* , pp. 15-16, 1999.

[41] S. L. Kim, "Rutile TiO2-modified multi-wall carbon nanotubes in TiO2 film electrodes for dye-sensitized solar cells," *Journal of Applied Electrochemistry* vol. 36, pp. 1433-1439, 2006.

[42] P. Wang, "Gelation of Ionic Liquid-Based Electrolytes with Silica Nanoparticles for Quasi-Solid-State Dye-Sensitized Solar Cells," *Journal of the American Chemical Society* vol. 125, pp. 1166-1167, 2003.

[43] D. Shi, "New Efficiency Records for Stable Dye-Sensitized Solar Cells with Low-Volatility and Ionic Liquid Electrolytes," *The Journal of Physical Chemistry C,* vol. 112, pp. 17046-17050, 2008.

[44] S. H. Kang, "Surface Modification of Stretched TiO2 Nanotubes for Solid-State Dye-Sensitized Solar Cells," *Journal of Physical Chemistry C* vol. 111, pp. 9614-9623, 2007.

[45] A. E. Curtright*, et al.*, "Expert Assessments of Future Photovoltaic Technologies," *Environmental Science & Technology* vol. 42, pp. 9031-9038, 2008.

[46] J. Mick. (2009, August 9th, 2009) "Cheap 'Popcorn Ball' Solar Cells Set Efficiency Record." *DailyTech*. Available: http://www.dailytech.com/article.aspx?newsid=11459

[47] F. Leonard, "Introduction," in *The Physics of Carbon Nanotube Devices*, ed Norwich: William Andrew Publishing, 2009.

[48] F. J. Owens and C. P. Poole Jr., "Carbon Nanostructures," in *The Physics and Chemistry of Carbon Nanosolids*, ed Hoboken: John Wiley & Sons, 2008.

[49] N. Yang*, et al.*, "Two-Dimensional Graphene Bridges Enhanced Photoinduced Charge Transport in Dye-Sensitized Solar Cells," *ACS Nano,* vol. 4, pp. 887-894, 2010.

[50] E. N. Pierce et. al., "Effects of Chronic Iodine Excess in a Cohort of Long-Term American Workers in West Africa," *The Journal of Clinical Endocrinology & Metabolism,* vol. 87, pp. 5499–5502, 2002.

[51] (11/12/2010). Acetonitrile. *MSDS Sigma-Aldrich - 271004,* 1-6.

[52] (11/12/2010). Valeronitrile. *MSDS Aldrich - 155098,* 1-6.

[53] (11/12/2010). 4-tert-Butylpyridine. *MSDS Aldrich - 142379,* 1-6.

[54] (11/12/2010). Terpineol. *MSDS Aldrich - 86480,* 1-5.

[55] (11/12/2010). 1-Butyl-3-methylimidazolium iodide. *MSDS Aldrich - 713066,* 1-5.

[56] L. Stryker. (2008, August 22nd, 2009) "Titanium Dioxide: Toxic or Safe?" Available: http://www.organicmakeup.ca/TitaniumDioxide.htm

[57] NIOSH, "Approaches to Safe Nanotechnology," DHHS, ed. Cincinnati, OH: DHHS (NIOSH), 2009, p. 86.

[58] (11/12/2010). Chloroplatinic acid hydrate. *MSDS Aldrich - 254029,* 1-6.

[59] (4/13/2010). Titanium(IV) chloride. *MSDS Fluka - 89541,* 1-6.

[60] M. K. Nazeeruddin*, et al.*, "A swift dye uptake procedure for dye sensitized solar cells," *Chem. Commun.*, pp. 1456-1457, 2003.

[61] Staples. (2010, November 21st, 2010) *Scotch 810 Magic Tape Refill, 3/4" x 27.7 yds. - 10/Pack*. Available: http://www.staples.com/Scotch-810-Magic-Tape-Refill-3-4-x-27.7-yds.-10-Pack/product_489211?cmArea=sku_pd_box2

APPENDIX

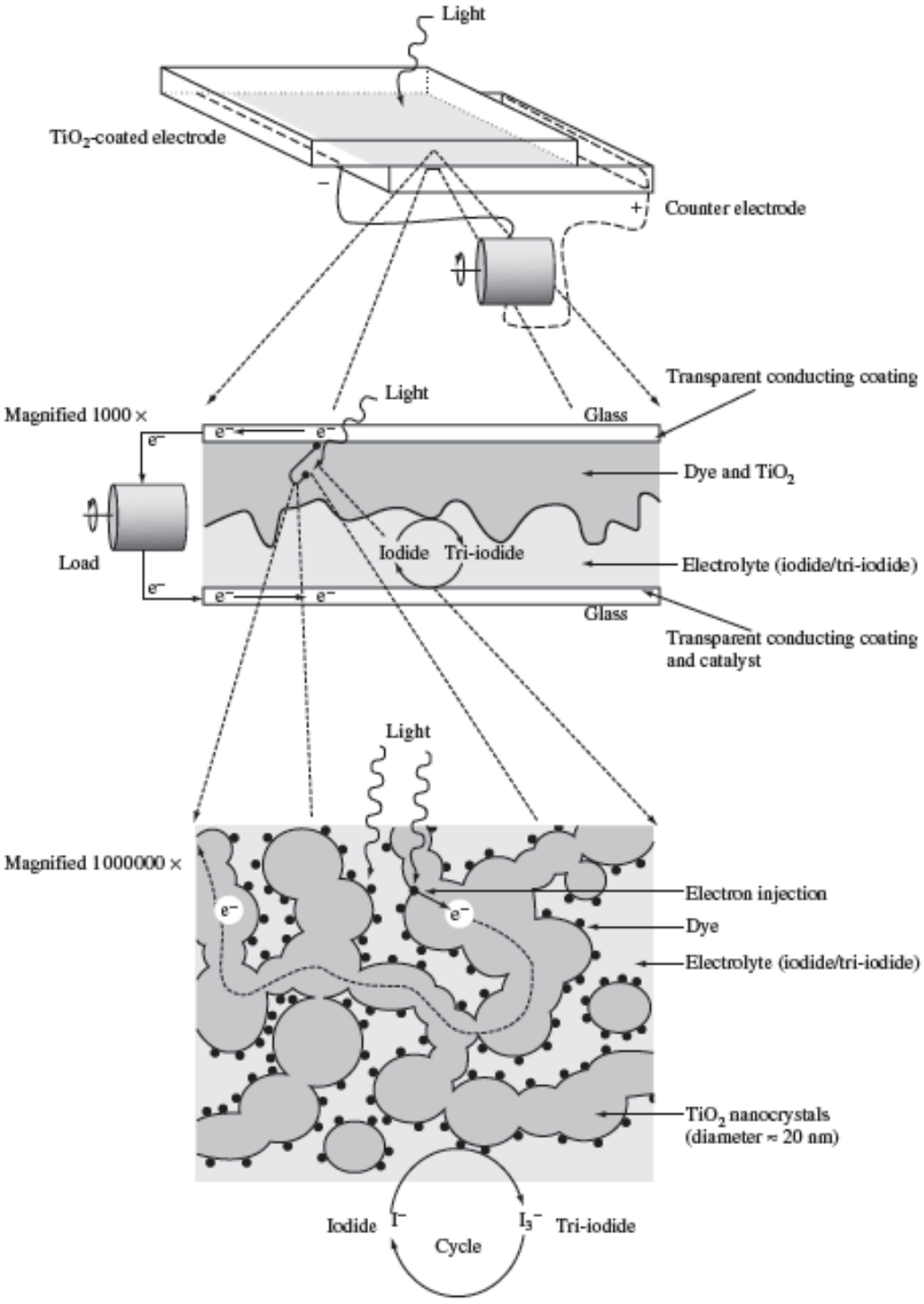

Plate 1: Diagram of DSSC arrangement and operation [10].

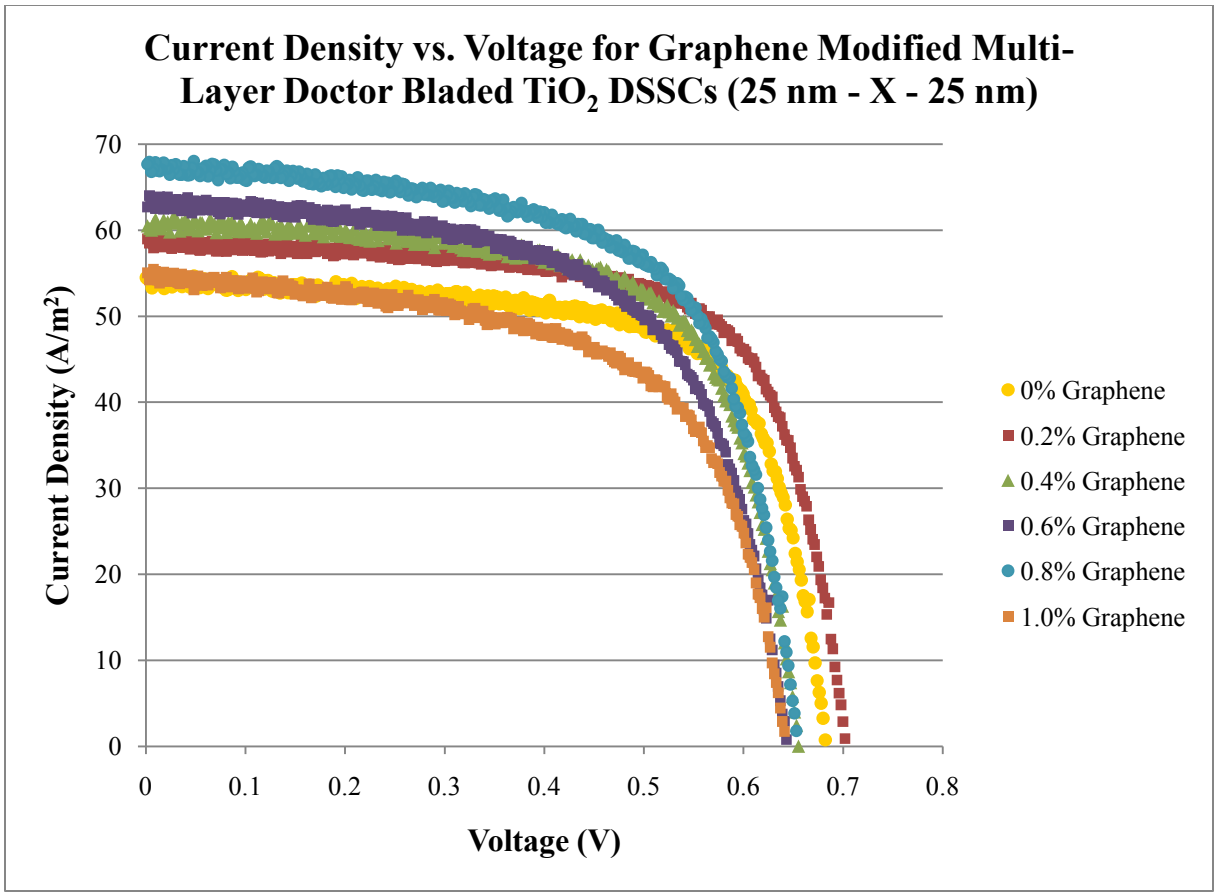

Figure 55: Testing results for multi-layer doctor bladed cells of the format 25 nm – X – 25 nm.

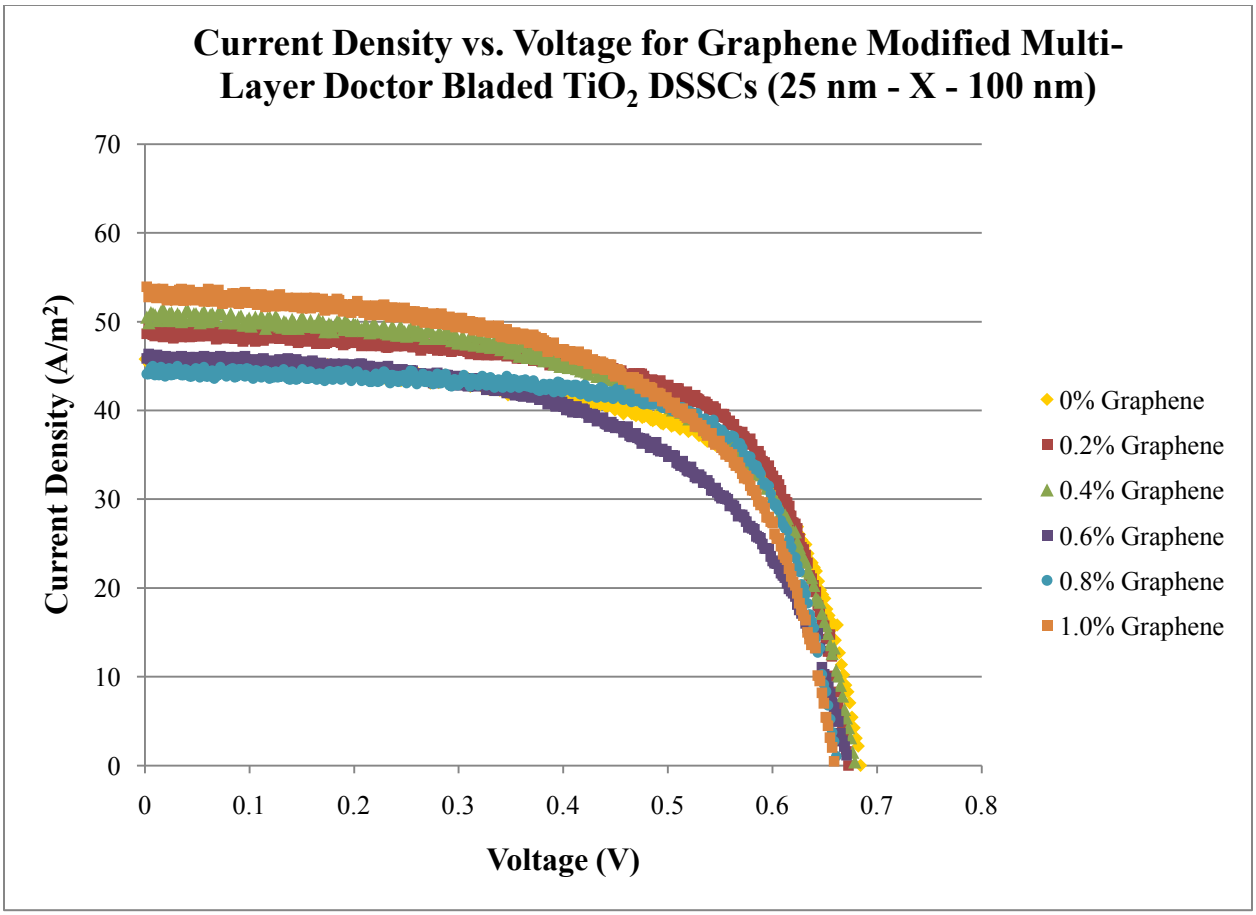

Figure 56: Testing results for multi-layer doctor bladed cells of the format 25 nm – X – 100 nm.

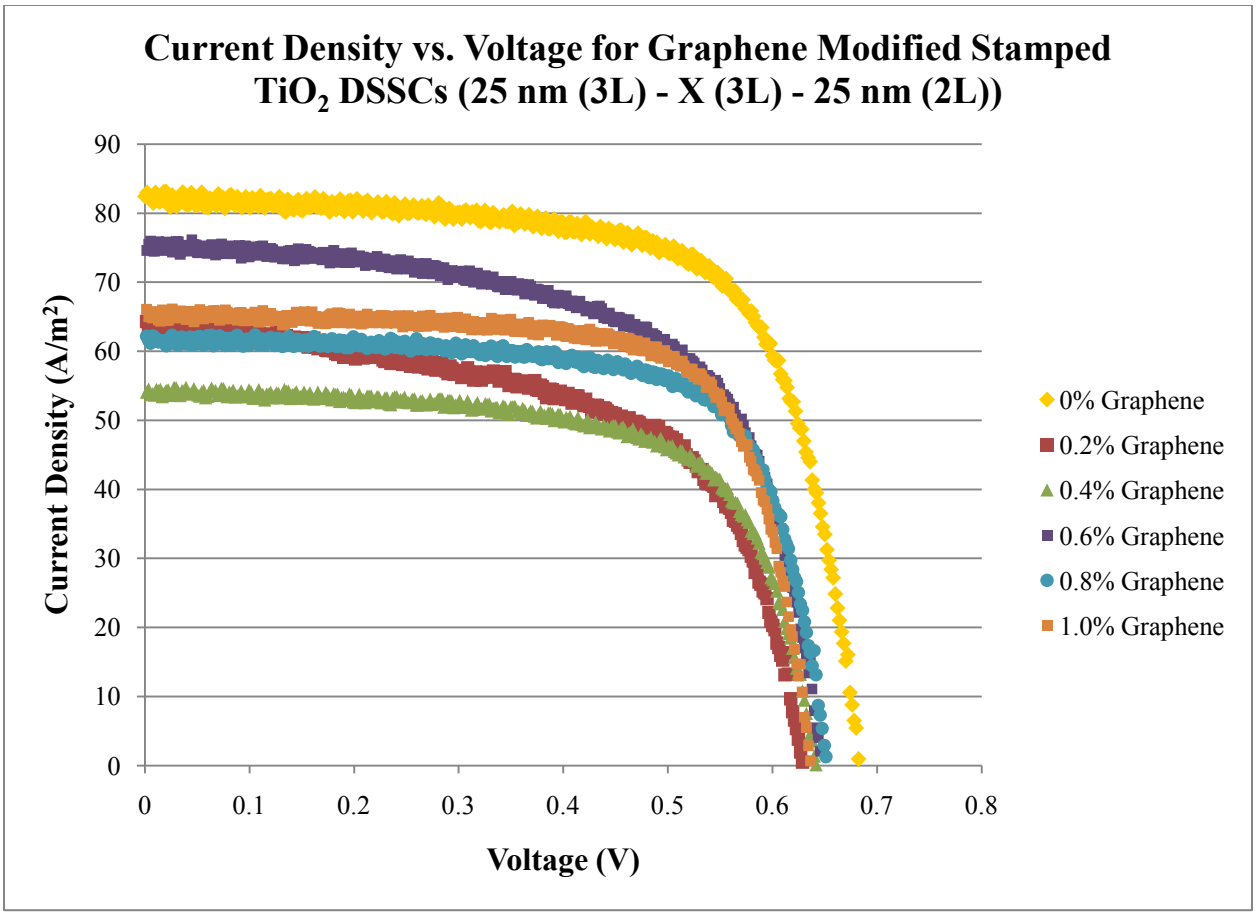

Figure 57: Testing results for 25 nm (3L) – X (3L) – 25 nm (2L) stamped cells.

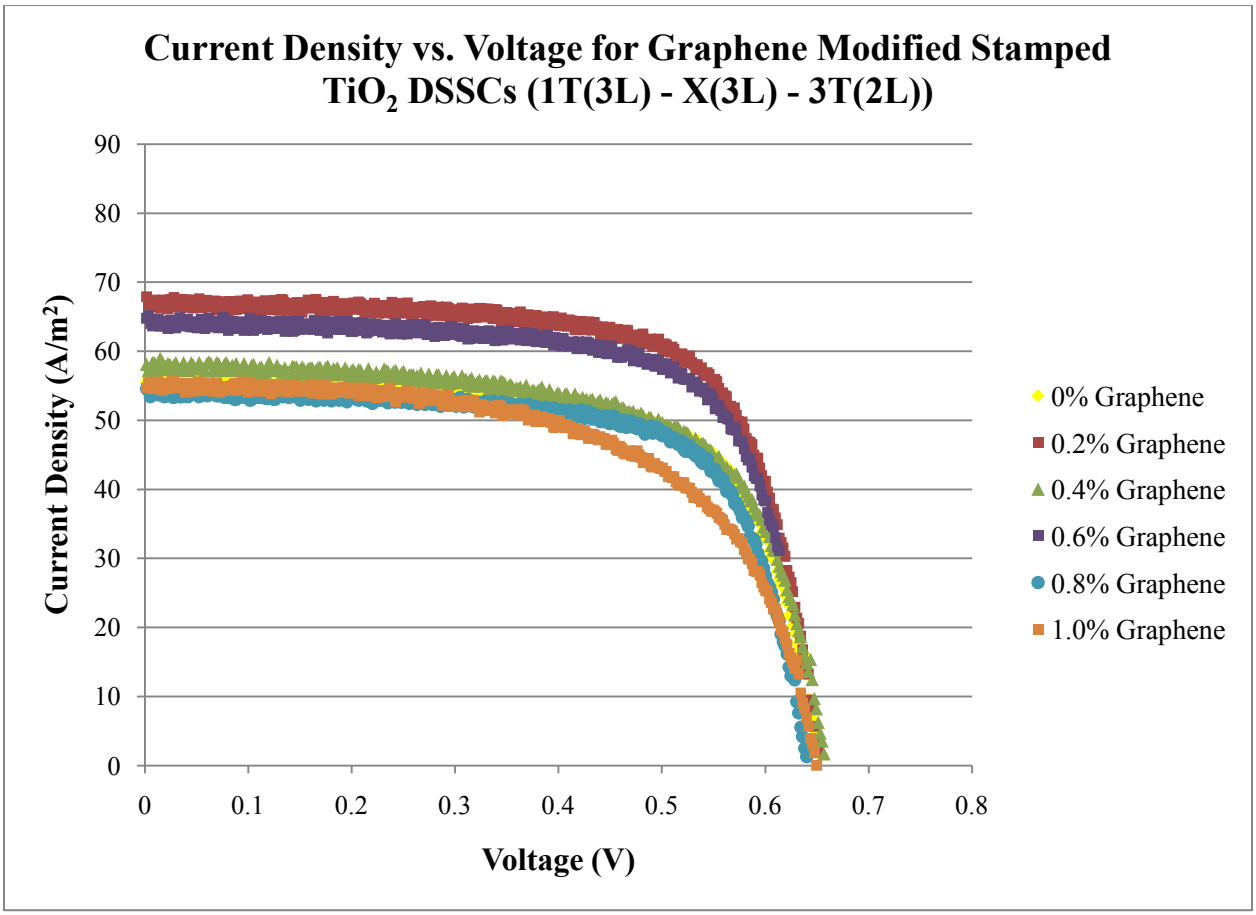

Figure 58: Testing results for 25 nm (3L) – X (3L) – 100 nm (2L) stamped cells.

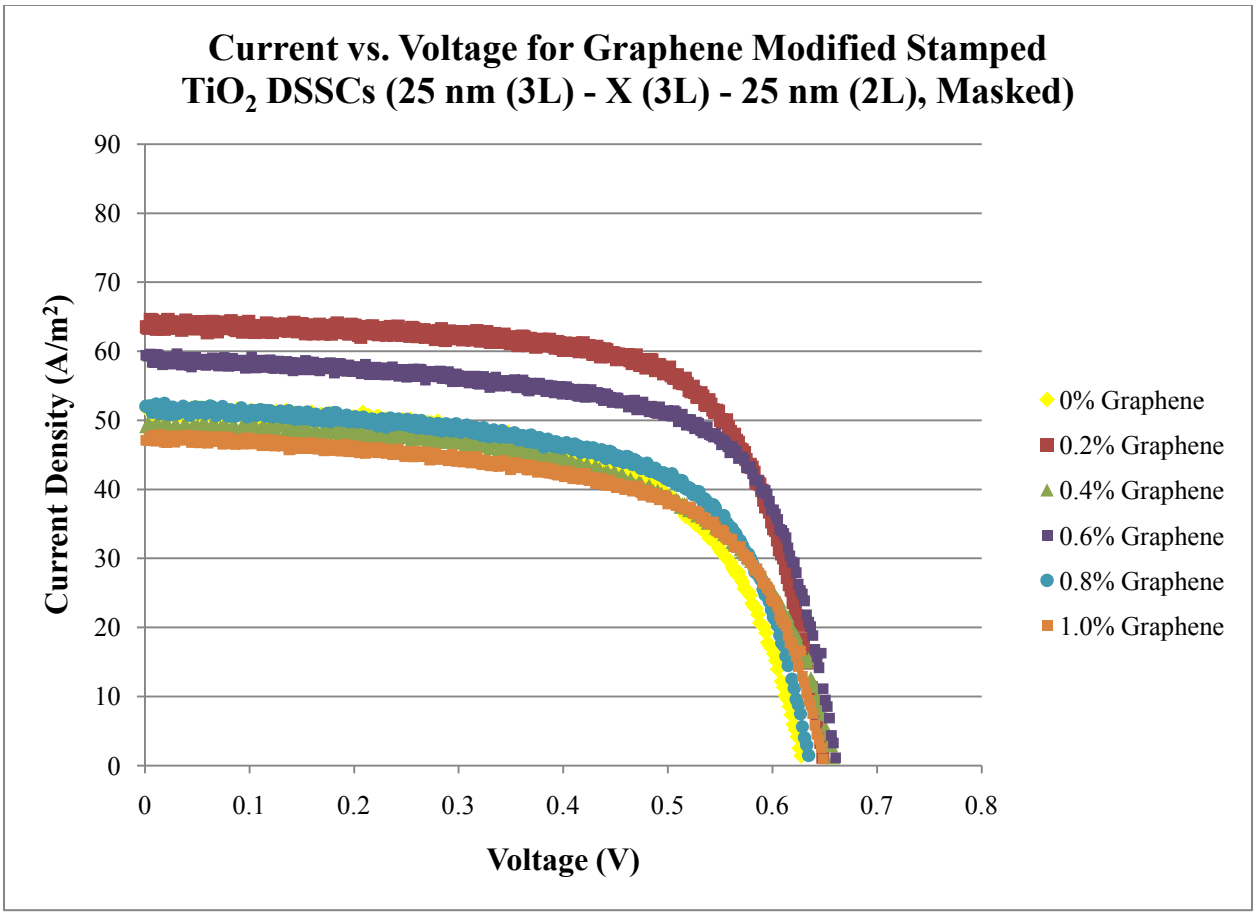

Figure 59: Testing results for 25 nm (3L) – X (3L) – 25 nm (2L) stamped masked cells.

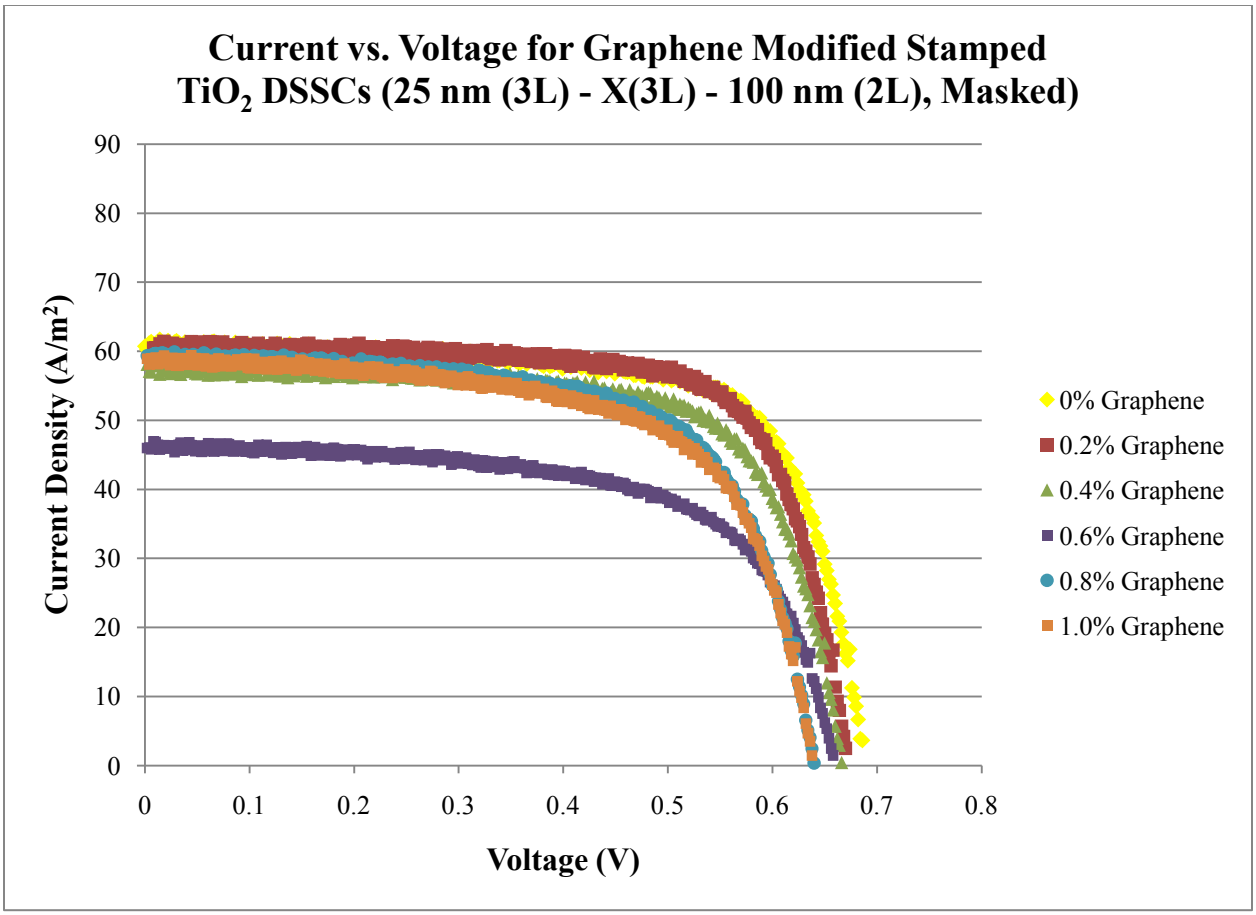

Figure 60: Testing results for 25 nm (3L) – X (3L) – 100 nm (2L) stamped masked cells.

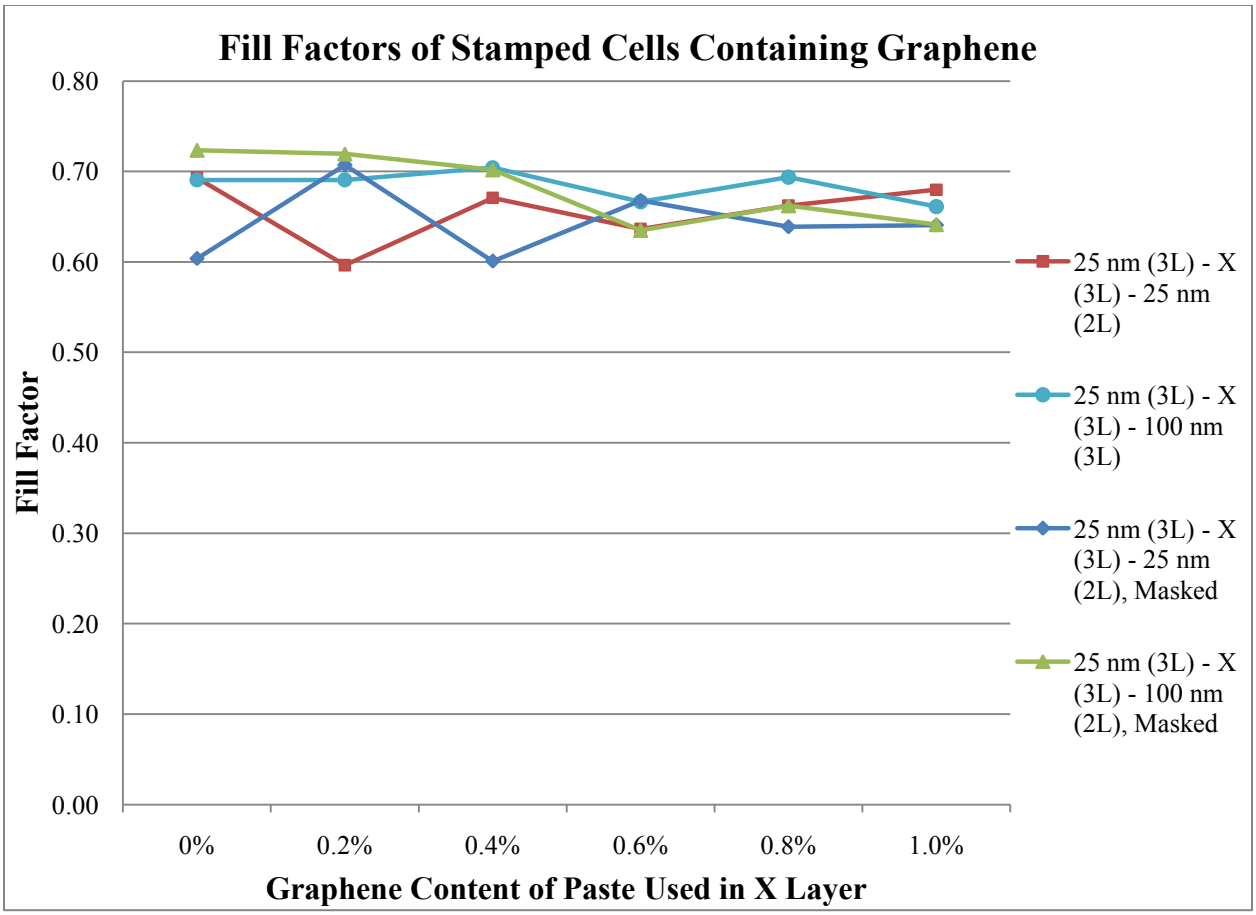

Figure 61: Fill factors of stamped cells containing graphene.

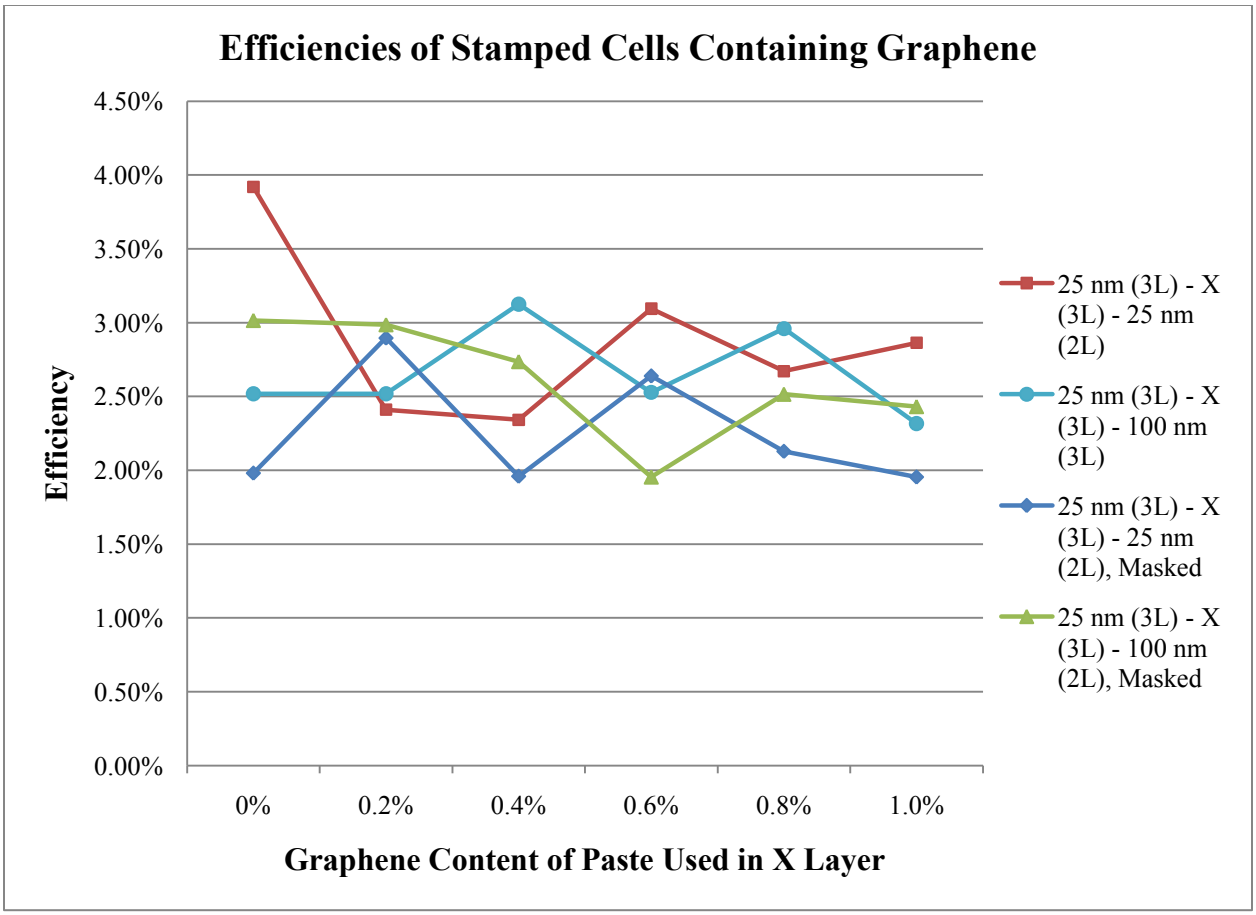

Figure 62: Efficiencies of stamped cells containing graphene.